

# Comparison of $\bar{N}N$ optical models

Jaume Carbonell<sup>a,1</sup>, Guillaume Hupin<sup>b,1</sup>, Slawomir Wycech<sup>c,2</sup>

<sup>1</sup>Université Paris-Saclay, CNRS/IN2P3, IJCLab, 91405 Orsay, France

<sup>2</sup>National Centre for Nuclear Research, Warsaw, Poland

Received: date / Accepted: date

September 27, 2023

**Abstract** We, compare the strong part of the  $\bar{N}N$  interaction obtained by the Nijmegen partial wave analysis and the results of some of the most popular  $\bar{N}N$  optical potentials in configuration space. We have found severe discrepancies in most of the partial waves, especially above  $p_{Lab}=400$  MeV/c where the partial wave analysis displays a resonant-like structure in the  $^{31}S_0$  and  $^{33}P_0$  waves. Some theoretical difficulties to interpret this behaviour in terms of dynamical resonances are pointed out and an alternative explanation is suggested. A much better stability is observed in the low energy parameters, apart from some discrepancies due to the presence of near-threshold quasi-bound states in particular waves. Large deviations have also been found between the corresponding potentials, at short and medium-range ( $r \gtrsim 1$  fm) distances.

**Keywords** Low energy antiproton physics · Optical models · Phase shifts PW analysis · Protonium

## 1 Introduction

In comparison with the Nucleon-Nucleon (NN) case, the Antinucleon-Nucleon- ( $\bar{N}N$ ) interaction remains poorly known. The reason for that is, on one hand the relatively limited number of  $\bar{N}N$  low-energy data and on the other hand the intrinsic difficulty of theoretically describing a system which has hundreds of open annihilation many-body channels at rest. See for instance [1,2,3] and references therein.

<sup>a</sup>e-mail: jaume.carbonell@ijclab.in2p3.fr

<sup>b</sup>e-mail: hupin@ijclab.in2p3.fr

<sup>c</sup>e-mail: Slawomir.Wycech@ncbj.gov.pl

A rigorous theoretical approach of this physical problem in its full complexity is far beyond our possibilities, both formal and computational, and it will remain so probably for a long time. There are however phenomenological ways to model the low energy  $\bar{N}N$  physics and obtain a reasonable description of the existing experimental data, provided one renounces to describe each particular annihilation channel and by introducing a relatively large number of parameters. A successful example is provided by the  $\bar{N}N$  optical models, which date from the early days of antiproton physics [4], and whose main properties have been recently reviewed in [5,6].

The first accurate description of the  $\bar{p}p$  experimental results was provided by the energy-dependent partial wave analysis of Nijmegen group [7] (NPWA) which presents an almost perfect description ( $\chi^2 \approx 1$ ) of the existing data below  $p_{Lab} < 925$  MeV/c, although after applying a severe rejection criteria. In this analysis, the long- and medium-range  $\bar{N}N$  interaction is given by a one- plus two-pion exchange potential ( $V_\pi \equiv V_{1\pi} + V_{2\pi}$ ) at N2LO chiral EFT detailed in [8]. This potential is matched at  $b=1.2$  fm to a state and energy-dependent complex boundary conditions which parametrise the short range physics, in particular the very complex annihilation dynamics. This is realised by fixing, for each energies  $E$  and partial wave  $\alpha = \{T, L, S, J\}$ , the logarithmic derivative of the corresponding wave function at  $r=b$ :  $P_\alpha(E)=b(\Psi'_\alpha/\Psi_\alpha)_{r=b}$ . The parameters of the NPWA, i.e. the low energy constants (LEC's) of  $V_\pi$  ( $c_1, c_3, c_4$ ) and the complex boundary conditions  $P_\alpha$ , were determined in [7] by a fit to the  $pp$  scattering data. The LEC's found in this way, were compatible with previous determinations from  $pp$  [8] and a combined fit of  $pp$  and  $pn$  scattering data [9].

The possibility of performing a PW analysis of the  $\bar{N}N$  data has been questioned [10,5], as it requires the determination of, at least, twice as many parameters as in the NN case, the number of  $\bar{N}N$  partial waves is higher than for NN, and the available  $\bar{N}N$  data are orders of magnitude less abundant. For instance, the  $\bar{N}N$  S-matrix for a tensor uncoupled states, is no longer determined by a real parameter  $\delta$  as in the unitary case ( $S = e^{2i\delta}$ ), but by a complex quantity  $\delta_C = \delta_R + i\delta_I$  whose (positive) imaginary part  $\delta_I$  controls the inelastic processes through the parameter  $\eta = |S| = e^{-2\delta_I}$  ( $0 < \eta < 1$ ), thus allowing the same formal expression for the S-matrix ( $S = e^{2i\delta_C}$ ). This criticism is sound and can eventually rise some questions about the uniqueness of the solution, especially when the inelasticity parameter  $\eta$ , and so the S-matrix itself, are very small. There is, however, no doubt that the results presented in [7] provide an excellent description of the selected data set and constitute at least one reliable solution in the domain  $100 \text{ MeV}/c < p_{Lab} < 1000 \text{ MeV}/c$ .

Once determined the parameters of the  $\bar{p}p$  PW analysis, the authors of Ref. [7] removed the Coulomb potential and the  $n - p$  mass difference ( $\Delta_0 \equiv m_n - m_p$ ), and obtained the strong  $\bar{N}N$  phase-shifts in the isospin symmetry, which are in fact the non trivial and interesting part of the interaction. These results, which can be considered to a large extent as being model independent, are extremely useful for a critical comparison between the different models, without directly relying on the experimental observables. The former, involve usually contributions of many partial waves and can hide eventual significant disagreements among the different interaction models. The strong  $\bar{N}N$  Nijmegen phase shifts constitute the basis of our further analysis.

The strong  $\bar{N}N$  phase-shifts provided by the Nijmegen group were also the starting point to determine the parameters of the most recent  $\bar{N}N$  Jülich potential [12]<sup>1</sup>. This potential is based on the G-parity transform of a previously established chiral EFT NN potential at N3LO [14]. It contains contributions from one- and two-pion exchange and of contact terms with up to four derivatives. The annihilation part is taken into account by introducing imaginary contact terms in each partial wave, regularized by gaussian form factors. The potential is inserted in a relativistic Lipmann-Schwinger equation to obtain the phase-shifts. The low energy constants of the pion-exchange part were taken from the

<sup>1</sup>It is worth mentioning that, under this denomination, one can include a series of previous works on  $\bar{N}N$  interactions developed since the 90's, based on the G-parity transform of the meson-exchange NN Bonn model [13] and even the N2LO version of the chiral EFT  $\bar{N}N$  potential [11]. For shortness of the notation, we will hereafter denote Jülich  $\bar{N}N$  potential as the one described in Ref. [12]

pion-nucleon dynamics and the remaining ones, as well as the annihilation constants, were adjusted to reproduce to the strong phase shifts and inelasticity parameters of the Nijmegen PWA in the isospin basis. Supplemented with the Coulomb and  $\Delta m$  term, this model provides an equally good description of the  $\bar{p}p$  data as in the NPWA. Furthermore it has been extended to describe the zero energy protonium results as well as the existing  $\bar{n}p$  data ( $T = 1$ ).

The Jülich potential constitutes nowadays the most complete and accurate description of the  $\bar{N}N$  data, would it be at the price of a considerable number of parameters ( $\approx 90$ ). However, it has been derived in momentum space what makes difficult its implementation to study more complex systems, in particular the very peripheral and loosely bound hydrogenic orbits of the  $\bar{p}$ -A systems. These Coulomb-like states constitute the cornerstone of the PUMA research project [15] that requires reliable theoretical predictions of the annihilation probabilities from some of them. A recent application to the simple  $\bar{p}$ -d case has been recently obtained [16] using a simplified (local) form of the Jülich potential. They led to significantly different predictions with respect to other existing models and it is not clear which part of these differences is a genuine prediction of the potential itself or results from the simplifications. On the other hand the strong non local character of the Jülich potential makes it difficult to be used in configuration space calculations, where the few-nucleon scattering problem can be more easily solved.

In view of further applications, but also for the sake of a theoretical consistency, it is of the highest interest to examine the predictive power of some of the most popular  $\bar{N}N$  optical models formulated in configuration space, by comparing them at the level of strong phase shifts as well as with the recent – phase equivalent – Nijmegen PW and Jülich results. A previous comparison devoted to protonium level shifts and scattering lengths was published many years ago [17,18] but to our knowledge no systematic study has been performed at non zero energies.

Our goal in the present paper is thus to establish a detailed comparison of the Nijmegen PW analysis and Jülich results with some selected optical models widely used in the literature and formulated in configuration space. To this aim we will consider the last updated version (2009) of the Paris potential [19], the Dover-Richard models [20,21] published in 1980-82 and the Khono-Weise [22] potential formulated in 1986. They represent different degrees of complexity in the theoretical description and, apart from being formulated in configuration space, they have in common that: (i) they make full use of conventional (not EFT) meson-

exchange theory, (ii) they were constructed before the NPWA [7], and (iii) they were adjusted to a restricted data set. At the end, they obtain a less accurate description of the experimental results than NPWA and Jülich model, but they use a much smaller number of parameters.

As we will see in what follows, there exist huge disagreements among the partial wave predictions of the considered optical models, often hidden when considering only integrated cross sections. They claim for an urgent clarification of the  $\bar{N}N$  interaction at the two-body level, both from the theoretical as well as from the experimental point of view, before intending a minimal model independent description of more complex systems, furthermore involving off-shell properties of the interaction.

We will sketch in section 2 the main ingredients of the theoretical  $\bar{N}N$  formalism used in Refs. [7, 12] as well as in our own calculations with Paris, DR and KW optical models. Section 3 is devoted to compare the strong phase shifts for the S and P partial waves, low energy parameters and S- and P-wave protonium level shifts of these different models. Section 4 contains some concluding remarks.

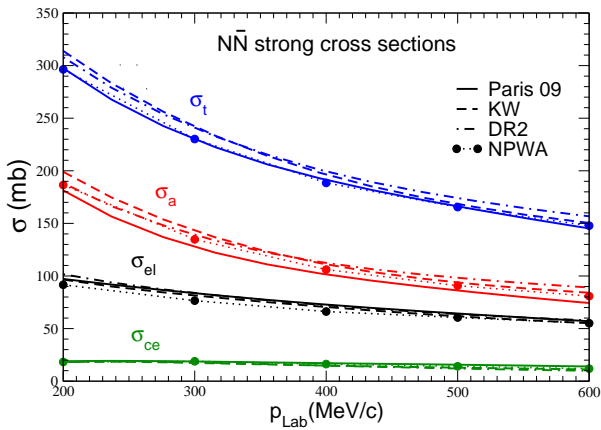


**Fig. 1** Integrated strong  $\bar{N}N$  cross sections – elastic  $\sigma_e$  (black), annihilation  $\sigma_a$  (red), charge-exchange  $\sigma_{ce}$  (green) and their sum  $\sigma_t$  (blue) – as functions of the  $\bar{N}$  laboratory momenta for DR2 (dashed dotted line), KW (dashed line) and Paris 2009 (solid line) optical models. The results of the Nijmegen Partial Wave analysis [7] are indicated by filled circles.

## 2 The formalism for $\bar{N}N$ optical models

The strong part of the  $\bar{N}N$  force is derived in the isospin basis ( $V_T$ ). However, this basis is not adapted to computing low-energy  $\bar{p}p$  scattering processes due to the relevant role of Coulomb interaction and, in a less extent, to the  $n$ - $p$  mass difference ( $\Delta_0 \equiv m_n - m_p$ ) which couples, even asymptotically, the isospin states. One uses, instead, the so called particle-basis where the  $|p\bar{p}\rangle$  and  $|n\bar{n}\rangle$  states are coupled only by the short range "charge-exchange" potential. By adopting the isospin conventions [23, 17]

$$N = \begin{pmatrix} p \\ n \end{pmatrix} \quad \bar{N} = \begin{pmatrix} -\bar{n} \\ +\bar{p} \end{pmatrix} \equiv \begin{matrix} |1/2, +1/2\rangle = -|\bar{n}\rangle \\ |1/2, -1/2\rangle = +|\bar{p}\rangle \end{matrix} \quad (1)$$

the particle basis is expressed in terms of  $\bar{N}N$  isospin states  $|T, T_3\rangle$  as

$$\begin{aligned} |p\bar{p}\rangle &= +\frac{1}{\sqrt{2}} \{|00\rangle + |10\rangle\} \\ |n\bar{n}\rangle &= +\frac{1}{\sqrt{2}} \{|00\rangle - |10\rangle\} \\ |p\bar{n}\rangle &= -|1, +1\rangle \\ |\bar{p}n\rangle &= +|1, -1\rangle \end{aligned} \quad (2)$$

The  $|p\bar{p}\rangle$  and  $|n\bar{n}\rangle$  states can be cast into a single state vector

$$|\Psi\rangle = \begin{pmatrix} \Psi_{p\bar{p}} \\ \Psi_{n\bar{n}} \end{pmatrix}$$

which, in the  $\bar{N}N$  models that we will consider, obeys the non-relativistic Schrodinger equation

$$(E - H_0) |\Psi\rangle = \hat{V} |\Psi\rangle \quad (3)$$

where  $E$  is the (non-relativistic)  $\bar{p}p$  energy in the center of mass. The potential matrix

$$\hat{V} = \begin{pmatrix} V_{p\bar{p}} & V_{ce} \\ V_{ce} & V_{n\bar{n}} \end{pmatrix} \quad (4)$$

is expressed in terms of the isospin components  $V_T$  and the  $\bar{p}p$  Coulomb potential

$$V_c(r) = -\frac{\alpha}{r}$$

as

$$V_{p\bar{p}} = V_{N\bar{N}} + V_c \quad (5)$$

$$V_{n\bar{n}} = V_{N\bar{N}} + 2\Delta_0 \quad (6)$$

$$2V_{N\bar{N}} = V_0 + V_1 \quad (7)$$

$$2V_{ce} = V_0 - V_1 \quad (8)$$

The kinetic energy is assumed to be channel-diagonal with the  $p$ - $n$  averaged mass  $m$

$$H_0 = -\frac{\hbar^2}{m} \Delta \quad m = \frac{m_p + m_n}{2} \quad (9)$$

After performing the PW expansion, the reduced radial wave functions  $u_i$  obey a set of  $n_c$  coupled differential equations

$$u_i'' + q_i^2 u_i - \sum_{j=1}^{n_c} v_{ij} u_j = 0 \quad (10)$$

where  $i, j$  encodes the channel indexes  $\{\bar{p}p, \bar{n}n\}$  as well as the quantum number  $\alpha = \{L, S, J\}$ ,  $q_i$  the channel momenta in the center of mass and

$$v_{ij} = mV_{ij}$$

We use natural units ( $\hbar = c = 1$ ) along the paper. For the tensor uncoupled states ( $^1S_0, ^1P_1, ^3P_0, \dots$ )  $n_c=2$  and for the tensor coupled ( $^3SD_1, ^3PF_2, \dots$ )  $n_c=4$ .

The relations between the channel momenta are obtained by assuming the same c.m. total energy ( $\sqrt{s}$ ), which leads to:

$$\frac{s}{4} = m_\alpha^2 + q_\alpha^2$$

This gives

$$q_{\bar{p}p}^2 = mE \quad (11)$$

$$q_{\bar{n}n}^2 = q_{\bar{p}p}^2 - 2\Delta_0 m \quad (12)$$

We will denote hereafter by  $q \equiv q_{\bar{p}p}$  the c.o.m. momenta of the  $\bar{p}p$  driving channel. Notice that when using the differential form (10), the  $n - p$  mass difference  $\Delta_0$  is already included in the channel momenta and must be removed from the potential (6).

In the numerical calculations we used  $m = 938.28$  MeV and  $\Delta_0 = m_n - m_p = 1.2933$  MeV. The  $\bar{n}n$  channel is open at the  $\bar{p}p$  center of mass energy  $E \geq 2.5866$  MeV, i.e.  $q = 0.2497$  fm $^{-1}$ . The relation with the laboratory momenta is given by

$$p_{Lab} = 2q\sqrt{1 + \left(\frac{q}{m}\right)^2} \approx 2q$$

that is  $p_{Lab} = 98.54$  MeV/c.

The strong  $\bar{N}N$  potentials that we have considered in this work take the form

$$V(r) = U(r) + W(r) \quad (13)$$

where real  $U$  is a G-parity transform of a NN potential regularised below some cut-off radius  $r_c$ , and  $W$  is the complex potential (eventually containing also a real part) accounting for the annihilation.

The Paris  $\bar{N}N$  model [19, 25, 26, 27] is based on the G-parity transform of the Paris NN potential [28, 29]. It contains one- and two-pion exchange (the latter via dispersion relations), plus  $\omega$  and  $A_1$  potentials as part of three-pion exchange. The real part  $U$  has a central, spin-spin, spin-orbit, tensor and quadratic spin-orbit terms. The first two are energy-dependent, what results into seven scalar amplitudes for a given isospin  $T$ . They are regularized below some distance  $r_c$  ( $r_c = 0.84$  fm or  $r_c = 1.0$  fm) by a cubic polynomial, whose coefficients introduce adjustable parameters. All together this gives nine parameters for each isospin. The annihilation potential  $W$ , derived in [24], is purely imaginary and has a similar spin structure as the real part. It

depends on six parameters for each  $T$ . A particularity of the Paris potential is the short range character of  $W$  ( $r_a = 1/2m_N \approx 0.1$  fm). The total number of parameters of the model is  $\approx 30$  and that ensures a fairly good description ( $\chi^2/\text{datum} \approx 5$ ) of most of the existing data, without any selection criteria, including differential cross sections and polarization observables.

In Dover and Richard models – DR1 version [20] and DR2 version [21] –  $U$  is taken from a simplified version of the NN Paris potential [28] containing  $\pi, 2\pi$  and  $\omega$  regularized below  $r_c = 0.8$  fm. DR models were adjusted to reproduce some analytic parametrisations of the total, elastic, charge-exchange and annihilation experimental integrated cross sections in the range  $0.4 < p_{Lab} < 0.9$  GeV/c with a  $\chi^2/\text{data} \approx 0.5$  for DR1. In addition to  $r_c$ , there are only four parameters which control the annihilation potential  $W$ .

In Kohno-Weise model [22],  $U$  is taken from the NN Ueda potential [30] with  $\pi, \rho, \omega, \sigma$  meson contributions, regularized below  $r_c = 1$  fm by a  $C^1$  matching to a Woods-Saxon potential. As for DR, the parameters come only from  $W$  and are adjusted to reproduce the  $\bar{p}p$  total ( $\sigma_t$ ), elastic ( $\sigma_e$ ) and charge exchange ( $\sigma_{ce}$ ) cross sections in the region  $200 < p_{Lab} < 700$  MeV/c. In this way this model provides a good description of the forward  $\bar{p}p$  elastic differential cross sections at  $p_{Lab} = 400, 500, 600$  MeV/c, and  $\bar{p}p$  elastic differential cross sections at  $p_{Lab} = 390, 490, 590$  MeV/c as well as of differential ce at 490 and 590 MeV/c. No  $\chi^2$  is given in this analysis.

In DR and KW models, the annihilation potential  $W$  is local, energy- and state-independent. It has the common form

$$W(r) = -\frac{W_0}{1 + e^{\frac{r-R}{a}}} \quad (14)$$

with the parameters given in Table 1.

	DR1	DR2	KW
$W_0$ (GeV)	21+20i	0.5+ 0.5i	1.2i
R (fm)	0	0.8	0.55
a (fm)	0.2	0.2	0.2

**Table 1** Parameters of the Dover-Richard (DR1 and DR2 versions) and Khono-Weise (KW)  $\bar{N}N$  optical models.

These three optical models differ by their meson contents, the value of the cut-off radius  $r_c$ , the regularization procedure as well as by their annihilation potentials. They generate the very different potentials presented in Appendix A. As an illustrative example, let us consider Figure 15 from this Appendix, corresponding to the real part of the  $^1S_0$  potentials. They

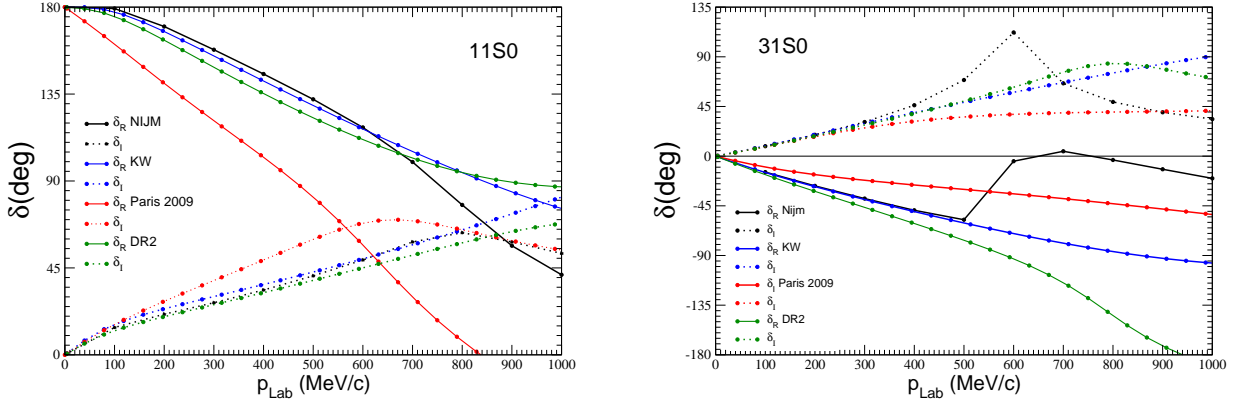


**Fig. 2**  $\bar{N}N$   $1^1S_0$  scattering phase shifts (degrees) as functions of the  $\bar{N}$  laboratory momenta and for different optical models. Left panel for  $T=0$  state ( $1^1S_0$ ) and right one for  $T=1$  ( $3^1S_0$ ). Solid lines correspond to the real part  $\delta_R$  and dashed lines to the (positive) imaginary part  $\delta_I$ .

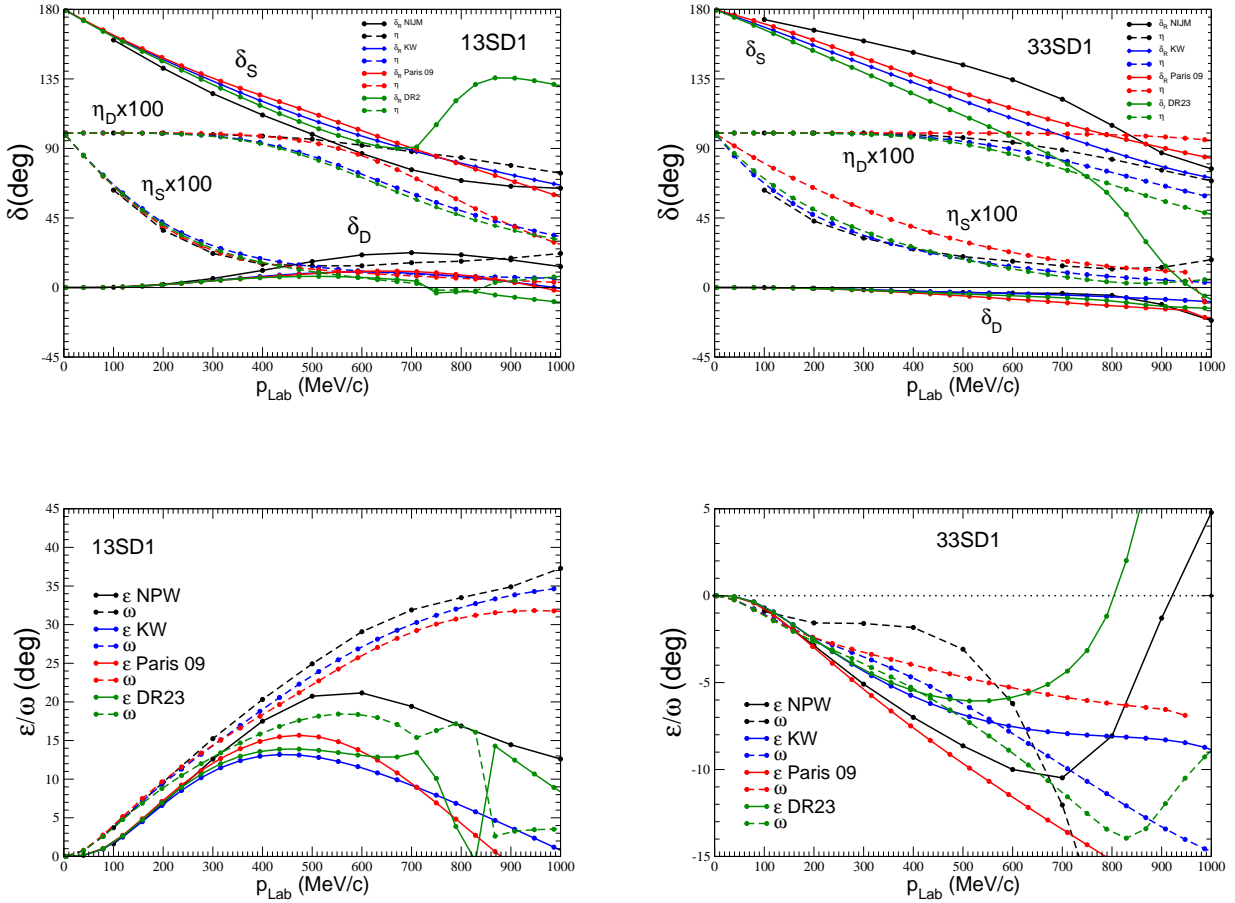


**Fig. 3**  $3^3S_1$   $\bar{N}N$  bare phase shifts and inelasticities (upper panel) and mixing parameters (lower panel), as functions of the  $\bar{N}$  laboratory momenta.

have in common a strong attraction (200-400 MeV at  $r = 0.8$  fm) in T=0 channel, which seems not required by the NPWA. On the other hand, the Paris potential displays a strong repulsion below  $r \approx 0.6$  fm as well as a repulsive barrier at  $r \approx 1$  fm that are absent in the other models. Despite of that, they provide quite similar results for the integrated elastic ( $\sigma_e$ ), annihilation ( $\sigma_a$ ) and charge exchange ( $\sigma_{ce}$ ) cross sections. This can be seen in Figure 1, where the integrated strong cross sections of these three models (together with their sum  $\sigma_t = \sigma_e + \sigma_a + \sigma_{ce}$ ) are compared to each other as well as to the NPW results [7]. The same agreement was observed in the protonium S- P- and D- level shifts and widths as well as for the strong and  $\bar{p}p$  scattering lengths (see Refs. [21,31,17,18]). However, no comparison has been done at the level of phase-shifts.

For the three considered models, Paris 2009, DR2 and KW, we have computed the S-matrix in the energy range  $0 < p_{Lab} < 1000$  MeV/c and for each PW state. We have extracted the S-matrix real parameters and compared them with the results of the Nijmegen PW analysis (Tabs VII-IX-X from Ref. [7]). The comparison with Jülich potential, adjusted to reproduce the former, would be redundant except for the low energy parameters that were not given in the NPWA [7] and that have been included in our discussion.

For the uncoupled states, the  $\bar{N}N$  S-matrix is determined by a complex phase shift  $\delta_C = \delta_R + i\delta_I$  whose (positive) imaginary part  $\delta_I$  is unambiguously defined by the modulus of the S-matrix, the inelasticity parameter  $0 < \eta < 1$ , according to

$$S = e^{2i\delta_C} = e^{2i\delta_R} e^{-2\delta_I} \quad \delta_I = -\frac{1}{2} \ln \eta \quad (15)$$

Notice that the annihilation cross section in a given PW, is entirely determined by  $\eta$  as

$$\sigma_a = (2J+1) \frac{\pi}{4q^2} [1 - \eta^2] \quad (16)$$

For the tensor-coupled states (e.g.  ${}^3SD_1$ ), the  $2 \times 2$  S-matrix can be parametrised by 6 real parameters – two "bare phase shifts"  $\delta_n$ , two mixing parameters  $\epsilon, \omega$  and two inelasticities  $\eta_n$  – according to the Bryan and Klarsfeld factorisation [32,33,34]

$$\begin{pmatrix} S_{11} & S_{12} \\ S_{21} & S_{22} \end{pmatrix} = \begin{pmatrix} e^{i\bar{\delta}_1} & 0 \\ 0 & e^{i\bar{\delta}_2} \end{pmatrix} M \begin{pmatrix} e^{i\bar{\delta}_1} & 0 \\ 0 & e^{i\bar{\delta}_2} \end{pmatrix} \quad (17)$$

where

$$M = \begin{pmatrix} \cos \epsilon & i \sin \epsilon \\ i \sin \epsilon & \cos \epsilon \end{pmatrix} H \begin{pmatrix} \cos \epsilon & i \sin \epsilon \\ i \sin \epsilon & \cos \epsilon \end{pmatrix} \quad (18)$$

and the matrix  $H$ , real and symmetric, contains the inelastic parameters  $\eta_i$  as eigenvalues

$$H = \begin{pmatrix} \cos \omega & -\sin \omega \\ \sin \omega & \cos \omega \end{pmatrix} \begin{pmatrix} \eta_1 & 0 \\ 0 & \eta_2 \end{pmatrix} \begin{pmatrix} \cos \omega & \sin \omega \\ -\sin \omega & \cos \omega \end{pmatrix} \quad (19)$$

Unitary models are defined by the condition

$$SS^\dagger = \mathbf{1}$$

to be fulfilled by (15) and (17). For uncoupled states, this implies  $\eta \equiv 1$  (or equivalently  $\delta_I \equiv 0$ ). For tensor-coupled states, this implies  $\omega = 0$ ,  $\eta_1 = \eta_2 = 1$  and so  $H = \mathbf{1}$ . In this case, (17) takes the usual Stapp-Ypsilantis-Metropolis (SYM) form defining the standard bare phase shifts  $\bar{\delta}_n$  and mixing parameter  $\bar{\epsilon}$  of the unitary case [35].

It is worth mentioning that, in the non unitary case, the definition of complex phase shifts for the coupled-channel states ( ${}^3SD_1, {}^3PF_2, \dots$ ) is not free from ambiguities. In fact, the inelasticity parameters can be negative: they are only limited by the so-called "unitarity condition" [33]

$$\text{Tr}(1 - SS^\dagger) = 2 - \text{Tr}(M^2) = 2 - \eta_1^2 - \eta_2^2 > 0$$

which presumes nothing about their sign. We have found that in some of the considered models one of the inelasticity parameters is indeed negative. This happens at relatively high energy, when the mixing angles  $\epsilon$  and  $\omega$  are large. The natural extension of the uncoupled case (15) to each inelasticity parameter  $\delta_{I,n} = -\frac{1}{2} \ln \eta_n$  poses a problem. There are alternative ways to define the complex phase shifts, e.g. the straightforward extension of the SYM parametrisation with complex parameters. However, though being totally consistent, the relation with respect to the previously defined parameters is not clear, even for the real part of the phase shifts. Again, the differences appears at large values of the mixing parameters, i.e. beyond the zero energy region. Because of that, the definition of the low-energy parameters (scattering length and effective range) remains unambiguous.

To get rid of this ambiguities, and to keep as closer as possible to the results of NPWA, we have only displayed in the tensor-coupled case the real bare shifts, together with the inelasticities and mixing parameters.

The practical determination of these parameters is more involved than in the tensor decoupled case and we have followed the procedure described in Sect VII of Ref. [7].

Together with the phase shifts, the corresponding effective range functions have been also computed and the corresponding Low Energy Parameters (LEP) have been extracted.

## 3 Results

### 3.1 Phase shifts

We first present the strong  $\bar{N}N$  complex phase shifts  $\delta_C = \delta_R + i\delta_I$  for the lowest partial waves as functions of

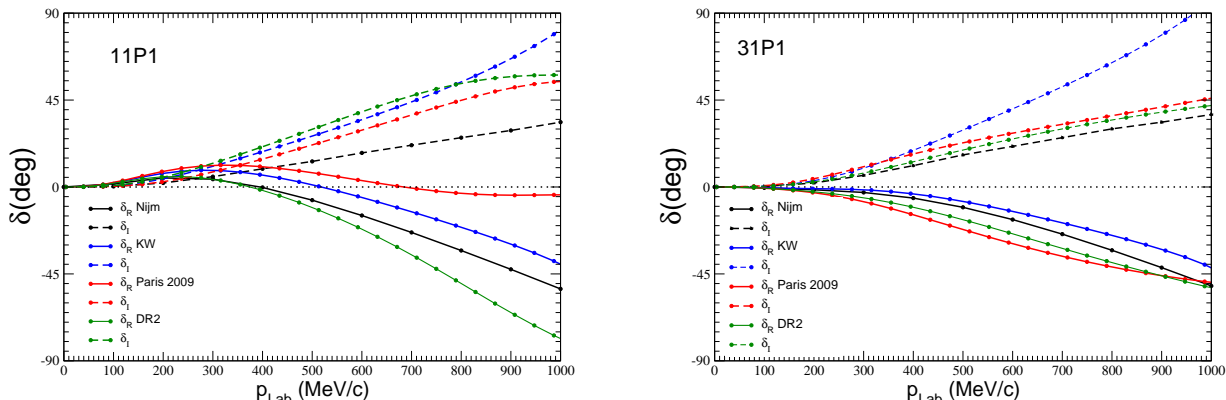


**Fig. 4**  ${}^1P_1$   $\bar{N}N$  scattering phase shifts as functions of the  $\bar{N}$  laboratory momenta. We use the same conventions as in Fig. 2.

the  $\bar{N}$  laboratory momentum  $p_{Lab}$ . The different states  $\alpha \equiv \{T, S, L, J\}$  are alternatively denoted in the spectroscopic notation by  $\alpha \equiv {}^{2T+1, 2S+1}L_J$ .

The values corresponding to Nijmegen PW analysis are taken from Tab. VIII of Ref. [7]. The other models KW, DR2 and Paris (2009) have been computed by the authors directly from the potentials, with the original model parameters. We emphasize that the Jülich model [12] results are, by construction, adjusted to the Nijmegen PW and there is no need to included them.

There is an  $\pm n\pi$  ambiguity in the definition of the phase shift  $\delta$  which is formally solved by imposing  $\delta(E \rightarrow +\infty) = 0$  and by keeping the same determination when the energy is decreased. Due to the sizable strengths of the  $\bar{N}N$  potentials, this recipe is however of little practical interest since it imposes to start with the solution at very high energy and go inwards in energy. In a unitary model (hermitian hamiltonian), another way to fix the determination is by imposing the value at the origin to be  $\delta_\alpha(E=0) = n\pi$ , where  $n$  is the number of bound states in channel  $\alpha$ . This impose the full knowledge of the spectrum for each partial wave. On the other hand, the validity of this result, known as Levinson theorem, is not well established in the non unitary systems like the optical models we are considering in this work. Thus, and for the sake of comparison, we have conventionally adjusted all the computed phase shifts to the determination given in the Nijmegen PW analysis [7].

**Figure 2 contains the results for the  ${}^1S_0$  state,** left panel for isospin  $T=0$  ( ${}^{11}S_0$ ) and right panel for  $T=1$  ( ${}^{31}S_0$ ). The real part  $\delta_R$  is in solid line and the (positive) imaginary part  $\delta_I$  in dashed line, both in degrees. Different colours have been used to disentangle the different models: black for the NPW, blue for KW,

red for Paris-2009. As one can see, there are major differences between them, specially in  $\delta_R$ , which deserve some comments.

For  $T=0$  state (left panel), the real phase shifts of KW and DR models are close to the NPWA ones up to  $p_{Lab} \approx 700$  MeV/c and they both depart dramatically from the Paris-2009 starting at very low energy. We recall the reader that the slope of the phase shift at the origin is the scattering length since  $\delta_\alpha(q) \approx -a_\alpha q$  where  $q$  is the center of mass momentum, related to  $p_{Lab}$  by  $p_{Lab} = 2q$ . This difference could be due to the fact that Paris potential has a near-threshold quasi-bound state in this channel, absent in KW and Jülich interactions. Its binding energy was  $E = -4.8 - 26i$  MeV in Ref. [19]. By using two independent methods, we confirm this state with a slightly different energy  $E = -10.2 - 23.2i$  MeV. As we will see in next subsection, the existence of this quasi-bound state is supported by a different sign in the corresponding scattering lengths (see Table 2). In this respect, a similar quasi-bound state is also present in DR2 model with  $E = -138 - 320i$  MeV, much deeper in energy and leaving no trace in the scattering region.

It is worth emphasizing, however, that there is no univocal relationship between the sign of the scattering length (real part) and the existence of bound states. For real potentials, the positive sign can be either a consequence of a repulsive interaction or of an attractive interaction having one (or several) bound states. The negative sign indicates always the existence of an attraction but tells us nothing about the existence or non-existence of a bound state, which will actually depend on the strength of the attraction. The situation is even more delicate when using complex potentials and additional informations are required to draw consistent conclusions.

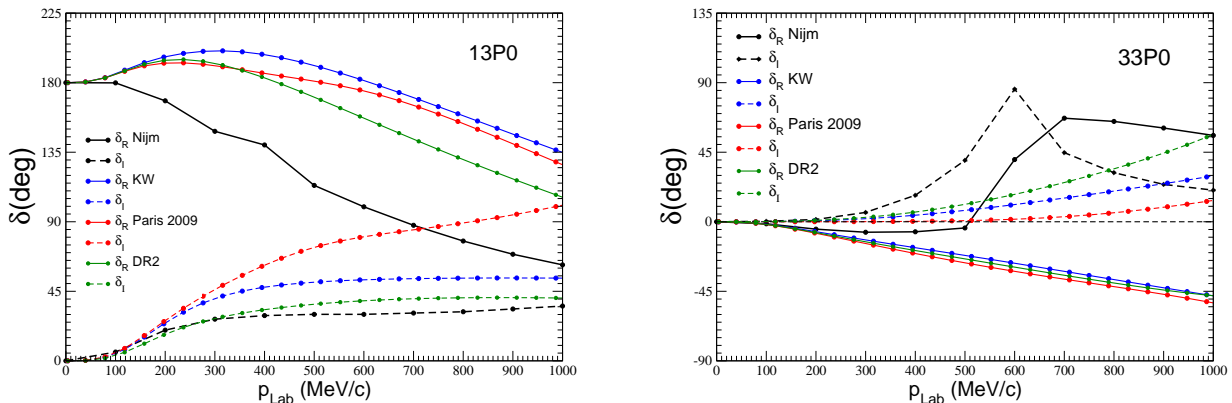


**Fig. 5**  ${}^3P_0$   $\bar{N}N$  scattering phase shifts (degrees) as functions of the  $\bar{N}$  laboratory momenta. We use the same conventions as in Fig. 2.

In particular, we would like to notice that the very existence of a quasi-nuclear state in the  ${}^1S_0$   $\bar{N}N$  state appears as a consequence of the sign of the measured  $\bar{p}p$  scattering length [38]. It was shown (See Figure 7 of this reference) that for weak (and attractive)  $\bar{p}p$  interactions – i.e. using large values of the cutoff radius,  $r_c > 1.7$  fm – the sign of  $\text{Re}[a_{\bar{p}p}]$  scattering length is negative. It becomes positive – and in agreement with experiment – only when, by decreasing  $r_c$ , the interaction is strong enough to create the first  $\bar{p}p$  bound state. The  $a_{\bar{p}p}$  involves however both isospin components and, from this single quantity, it is not possible to conclude in which of the component it appears. Notice also that the properties of such states, in particular their width, strongly depend on the annihilation dynamics. When using short range annihilation potential, as in Paris potential and in some coupled-channel unitary models (UCCM), the widths are much smaller than when using annihilation potentials type eq. (14), as in DR2, KW and Jülich potentials. One can find a discussion in Refs. [41] for KW and [38] for UCCM.

The particular E-dependence of the Paris potential in the  ${}^1S_0$  state is also observed in the imaginary phase shift  $\delta_I$ , which remains in a reasonable agreement with other models only up to  $p_{Lab} \approx 200$  MeV/c and displays a maximum at  $p_{Lab} \approx 600$  MeV/c.

When studying the  $J/\Psi \rightarrow \gamma p\bar{p}$  decay of BES collaboration, the authors of Ref. [36,37] interpreted the first peak in the  $\bar{p}p$  invariant mass in terms the above mentioned  ${}^1S_0$  quasi-bond state, and the second one in terms of a resonant state  ${}^1S_0$  at  $\approx 250$  MeV above the threshold, i.e.  $p_{Lab} \approx 950$  MeV/c. The peculiar form of the Paris  ${}^1S_0$  potential depicted in Fig. 15, displaying a deep attractive well and repulsive pocket at  $r \approx 1$  fm,

can indeed accommodate an S-wave resonance, but the height of the repulsive barrier is two times smaller than the supposed resonance energy. On the other hand, no clear evidence of this state is seen in the corresponding phase shifts. Only a vague structure is noticeable in  $\delta_R$  (red solid line) in the vicinity of  $p_{Lab} \approx 600$  MeV/c, with a maxima of  $\delta_I$  at almost the same energy, that could be related.

For T=1 state (right panel), the same discrepancy in  $\delta_R$  between the Paris result and the other models is observed. However there is a major difference between the NPWA and the other optical models: the sharp resonant-like structure that the former manifests at  $p_{Lab} \approx 600$  MeV/c, both in the real and in the imaginary phase shifts. The existence of an S-wave shape resonance would require a  ${}^3S_0$  potential with a repulsive bump at finite distance, like for instance the one exhibited in Figure 15 for the Paris 2009 model, in the T=0 channel. But none of the considered models exhibit such a behaviour (See Appendix).

The possibility for the NPWA to generate a resonance in this partial wave with a purely attractive (single-channel) potential is difficult to understand. Indeed, in their analysis the long- and medium-range part of the  $\bar{N}N$  interaction was parametrized by the one-pion ( $V_{1\pi}$ ) plus the two-pion ( $V_{2\pi}$ ) exchange potentials. According to the recent work from the Idaho group on the EFT-NN interaction at N3LO [39],  $V_{2\pi}$  for S=0 states is strongly attractive in both isospin channels, in agreement with previous works [40]. Let us remind that when going from NN to  $\bar{N}N$  system,  $V_{1\pi}$  contribution change the sign while  $V_{2\pi}$  remains unchanged.

We have displayed in Figure 6 the  $V_{1\pi}$  and  $V_{2\pi}$  contributions to  $\bar{N}N$  potential in spin singlet states for



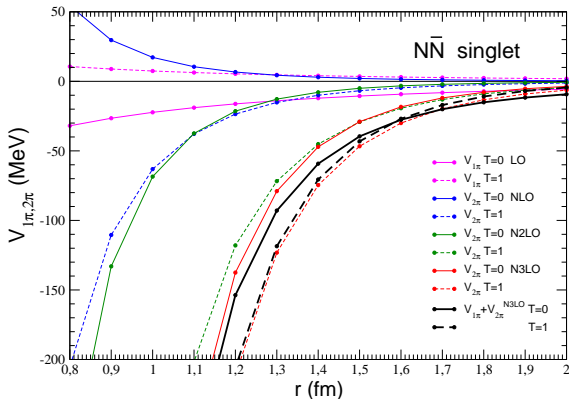


**Fig. 6** One- ( $V_\pi$ ) and two-pion ( $V_{2\pi}$ ) exchange potentials in singlet  $\bar{N}N$  states. Results are taken from G-parity transform of the EFT inspired NN Idaho potential [39]. The different orders up to N3LO, are plotted separately for both isospin (T) channels. The sum  $V_\pi \equiv V_{1\pi} + V_{2\pi}$  is strongly attractive. Only the T=0 states at NLO shows a short range repulsion.

both T components. As one can see, the only repulsion appears for T=0 at NLO, as in Paris potential, but becomes increasingly attractive at higher orders. In NPWA, the attractive pion tail ( $1\pi + 2\pi$ ) is prolonged at  $b = 1.2$  fm with a boundary condition corresponding to an also attractive square well (see Tab 1 from [7]). Thus, the overall  $^{31}\text{S}_0$  potential is attractive, as it is the case of the other (KW, DR2, Paris) examined potentials. See Figure 15 in the Appendix. Furthermore the resonant-like bump takes place at center of mass energy of  $E \approx 100$  MeV, which is quite a high energy for a single-channel S-wave to produce a visible bump in the phase shifts.

It must be pointed out that other mechanism to mimic resonant like structures in S-wave exist. For instance when a bound state, generated by the real part of the interaction, moves into the positive energy region due to the annihilation potential. The trajectory from the bound state to the continuum region in the complex energy plane was examined in our previous work with the KW potential [41]. This can be illustrated by the complex energy trajectory of the  $^{11}\text{S}_0$  state as function of the annihilation strength  $W_0$ . When  $W_0 = 0$  there is a bound state at  $E = -54.7$  MeV. When the annihilation is switched on, its imaginary part of the energy increases linearly with  $W_0$  and the state is pushed out into the continuum. It reaches  $\text{Re}(E) > 0$  at  $W_0 \approx 0.47$  GeV and has a width  $\Gamma \approx 230$  MeV. The energy imaginary part continues to increase until the model value  $W_0 = 1.2$  GeV. Thus, the widths of the positive energy

states ( $E \sim 100$  MeV) thus obtained within this mechanism are very large (few hundreds of MeV) and cannot generate structures like the one displayed in the right panel of Fig. 2.

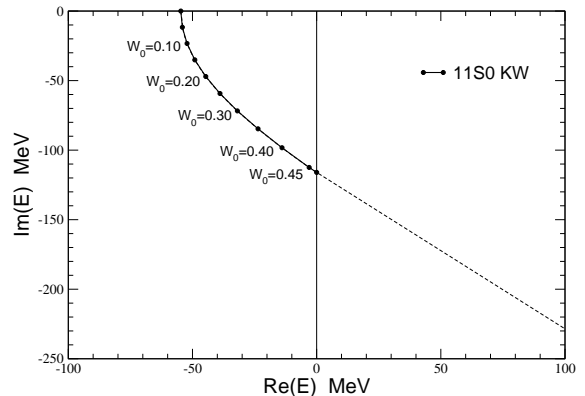


**Fig. 7** Pole trajectory of a  $^{11}\text{S}_0$  bound state in KW model as function of the strength of the imaginary part  $W_0$ . In absence of annihilation potential ( $W_0 = 0$ ), there is a bound state with  $E = -54.7$  MeV. The effect of the annihilation potential is to generate a width and to pull out the state into the continuum. When  $W_0 \approx 0.47$  GeV, one has  $\text{Re}(E) = 0$  and  $\text{Im}(E) \approx 115$  MeV. With the model parameter  $W_0 = 1.2$  GeV, the width of the state is  $\sim 400$  MeV.

All these reasons above, make it difficult to understand the structure displayed in Figure 2 (right panel) in terms of a resonance in the  $^{31}\text{S}_0$  PW, especially at 100 MeV above threshold.

On the other hand, it is worth noticing that the Jülich potential nicely reproduces the  $^{13}\text{S}_0$  phase shifts of the NPWA, that was attributed to an S-wave resonance, although no further explanation in terms of the underlying potential was given in their manuscript. This is a non trivial achievement, that worked also reasonably well in their N2LO version [11], and shows the extreme flexibility of the EFT potential.

Interestingly, the same group, came to the conclusion [42, 43] that in order to reproduce the BES results on the  $J/\Psi \rightarrow \gamma p \bar{p}$  decay they were forced to slightly modify their original  $^{31}\text{S}_1$  potential. Once readjusted, the corresponding phase shifts do not reproduce anymore the NPWA structure of Figure 2 (right panel) but are very close to the – smoothly varying – KW results (blue curve). This happens in the N2LO [11] as well as in the N3LO versions of Jülich potential [12]. The authors conclude that the origin of the near-threshold peaks observed in the BES experiment, may be ex-

plained by assuming the existence of a  $\bar{N}N$   $^1S_0$  quasi-bound state, but in the  $T=1$  rather than in the  $T=0$  channel, as claimed in [36, 37]. Its energy was estimated to be  $E = -36.9 - 47.2i$  MeV. It could be relevant to notice that all the examined models have indeed a bound state in this PW when  $\text{Im}(V)=0$ . The imaginary part of the potential pushes KW one into continuum while the DR2 and Paris ones remain still bound, although sizeably deeper than in the Jülich potential :  $E=-430-346i$  MeV for DR2 and  $E=-184-171i$  MeV for Paris.

The possible origin of the resonant-like structure manifested in the NPWA, which is also manifested in other partial waves, will be discussed later.

Our last comment on this  $^1S_0$  state, is to remark that the imaginary phase shifts  $\delta_I$  agree reasonably well with each other up to  $p_{Lab} \approx 400$  MeV/c, where the resonant-like behaviour of the NPWA starts showing up.

**Figure 3** displays the S-matrix bare phase shifts and inelasticities (upper panel) and the mixing parameters (lower panel) of the triplet tensor coupled  $^3SD_1$  state. The  $^3S_1$  bare phase shifts  $\delta_S$  seem to be more stable than the  $^1S_0$  ones, for both isospin states, although in this case the best agreement is among KW, DR2 and Paris.

For  $T=0$ , the bare shifts  $\delta_S$  are very close to each other up to  $p_{Lab}=700$  MeV/c, where DR2 displays some structure, crossing 90 degrees in increasing, what suggest a standard resonance driven by D-waves due to its centrifugal barrier. The same structure is manifested in  $\delta_D$  and the mixing parameters. The inelasticities are less stable:  $\eta_S$  (left panel) departs sharply from NPW at  $p_{Lab} \approx 500$  MeV/c while  $\eta_D$  the dispersion among the models starts already at  $p_{Lab} \approx 300$  MeV/c. The mixing parameter  $\epsilon$  shows also strong deviations above 300 MeV/c while  $\omega$ 's are relatively close to each other.

For  $T=1$  (right panel) the S-wave inelasticity of Paris potential departs sensibly from the other models from the zero energy region. The dispersion in the mixing parameters is huge, with NPW and DR23 displaying a peculiar energy dependence.

**The  $^1P_1$  phase shifts are displayed in Fig. 4**, using the same line and colour conventions as in Fig. 2. At first glance, it seems that in this case the global behaviour of the models is quite similar, at least at low energy. However, we will see in the next section that this is not really the case: major deviations exist from the origin but these differences are hidden in this representation due to  $q^3$  behaviour at small  $q$ .

**The  $^3P_0$  results are displayed in Fig 5**, with the same colour convention as in Fig. 2 and 4. In this partial wave, the differences between the model predic-

tions (KW, DR2 and Paris-2009 ) – relatively close to each other – and the results of the NPWA are dramatic.

For  $T=0$ , the deviations in  $\delta_R$  start already at  $q \approx 0$ , displaying a different concavity. This corresponds to a negative effective range for the NPW (see Table 3). The imaginary phase shifts  $\delta_I$ , start differing at  $p_{Lab} = 200$  MeV/c and the differences increase with the energy.

For  $T=1$ , the low energy phase shifts of all models are quite in agreement, including NPW results, what is manifested in the LEP's displayed in Table 3. Deviations start above  $p_{Lab} = 200$  MeV/c, where the NPW results display the same resonant-like structure that the one observed in the  $^3S_0$  state, and practically at the same value of  $p_{Lab}$ .

Contrary to the  $^3S_0$  case, the  $^3P_0$  potential has a centrifugal barrier which can indeed accommodate a resonance, provided that the interaction is attractive enough. However, it is not the case in any of the examined models – KW, DR2 and Paris – which are globally repulsive in this channel (See Fig. 19 from the Appendix). This is in agreement with the corresponding scattering volumes in Table 3, including the values of the Jülich potential : they are very stable and have very small imaginary parts, as it corresponds to a repulsive interaction. Nevertheless, the inner part of the NPW potential, used to define the boundary conditions at  $b=1.2$  fm, is an attractive square well with 160 MeV depth. Even if beyond  $r = b$  the long range part  $V_\pi$  is slightly repulsive, the effective potential ( $V+$  centrifugal) in the vicinity of  $r = 1$  fm remains globally attractive ( $-80$  MeV) and we cannot exclude that a resonance could indeed be produced.

This will be in strong tension with all the potentials, but this is not the only reason to be cautious with such a possibility. On one hand the maximum of the centrifugal barrier (60 MeV at  $r=1.2$  fm) is sensibly smaller than the resonance energy ( $p_{Lab} = 600$  MeV/c,  $E_{cm} \approx 95$  MeV). On the other hand, the  $\delta_R$  and  $\delta_I$  curves of both  $T=1$  states,  $^3S_0$  and  $^3P_0$ , can be overimposed in the vicinity of the peak. Since it is difficult to attribute such a coincidence to a dynamical effect, occurring in two independent PW at the same energy, this behaviour suggest to look for an alternative explanation. We will come back to this important point at the end of this section.

**The  $^3P_1$  results are displayed in Fig 8** with the colour convention of the previous Figures. For the  $T=0$  state (left panel), all the phase shifts display quite a similar behaviour up to 300 MeV/c but the considered optical models start to depart dramatically from NPWA at  $p_{Lab} \approx 400$  MeV/c. Below that, it is one of the most stable channels.

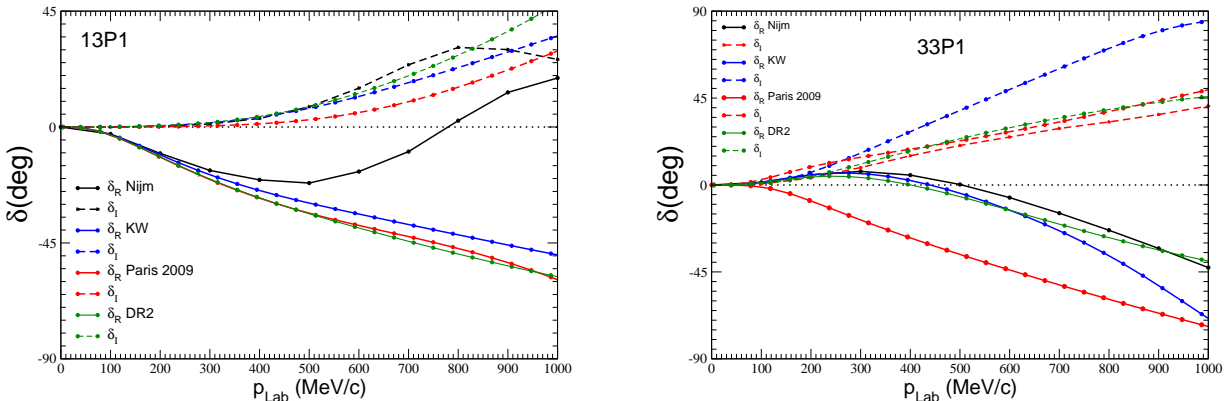


**Fig. 8**  ${}^3P_1$   $\bar{N}N$  scattering phase shifts (degrees) as functions of the  $\bar{N}$  laboratory momenta, using same conventions than in Fig. 2

For  $T=1$  (right panel), the deviations are more sizeable already from the zero energy region, specially in  $\delta_R$  with Paris 2009. This difference is due to the existence of a near-threshold quasi-bound state with  $E = -3.6 - 12.42i$  MeV, (slightly different from the value  $E = -4.5 - 9.0i$  MeV given in [19]) that is absent in the other models and is responsible for a different sign of the scattering volume (see Table 3).

Finally, we show in Figure 9 the bare phase shifts and mixing parameters for the  ${}^3P_2$  partial wave.

For  $T=0$ , and in spite of some stability in the scattering lengths, the results of  $\delta_P$  falls in two different families: on one side the NPW and DR2 which are attractive and on the other KW and Paris that are repulsive. This qualitative difference remains such in all the considered energy domain. The same splitting is observed in the mixing parameters above  $p_{Lab} \approx 200$  MeV/c.

For  $T=1$ , a similar situation happens, with the  $\delta_P$  values of NPW evolving in the opposite direction than the rest of the models. Remarkably, the mixing parameter  $\epsilon$  remains stable up to  $p_{Lab} \approx 600$  MeV/c while  $\omega$  values start diverging at 300 MeV/c.

As we already mentioned, the NPW results for the  ${}^{31}S_0$  and  ${}^{33}P_0$  states, display the same kind of non trivial structure at  $p_{Lab} \approx 600$  MeV/c both for the real and the imaginary phases, while they are absent in the examined optical models, with the exception of Jülich potential which reproduces it well. It seems however unlikely, although not impossible, that a dynamical effect could generate two resonances at the same energy, in different partial waves having the same parameters, one in S-wave and other in P-waves.

Looking for a possible explanation of these structures, we noticed that this energy region corresponds to a sharp maximum of  $\delta_I$ , that is to a minimum of the inelasticity parameter  $\eta$ , which turns to be – in this particular waves – very small. For the  ${}^{31}S_0$ , for instance, one has  $\eta \approx 0.01$  at the minima, that is one order of magnitude smaller than for the  ${}^{11}S_0$ . The same is true for the  ${}^{33}P_0$  state, when compared to other P-waves. This can be seen in Fig. 10, where the inelasticity parameter  $\eta$  is plotted as function of  $p_{Lab}$  for several states and where the peculiarity of the  ${}^{11}S_0$  and  ${}^{33}P_0$  states is manifested.

Since

$$|S_\alpha(E)| = e^{-2\delta_I^\alpha(E)} = \eta_\alpha(E)$$

the scattering matrix of  ${}^{11}S_0$  is in modulus  $\sim 10^{-2}$ . And similar values for the  ${}^{33}P_0$  one.

Given the (not estimated) errors of the PW results in the region of the resonant-like structure, the S-matrix of these particular waves is in fact compatible with zero, quite a different situation than for a real resonance where the S-matrix would have rather a pole. It corresponds actually to the "black sphere model" scattering, which is quite different from a resonant scattering, although it produces indeed some structure in the phase shifts.

It remains to be seen whether these structures are an artefact of the analysis or if they remain unavoidable conclusions of it.

In this respect, it could be pertinent to notice that both states where they occur are  $J = 0$ , they have very little statistical weight and could be affected by large errors in their determination.

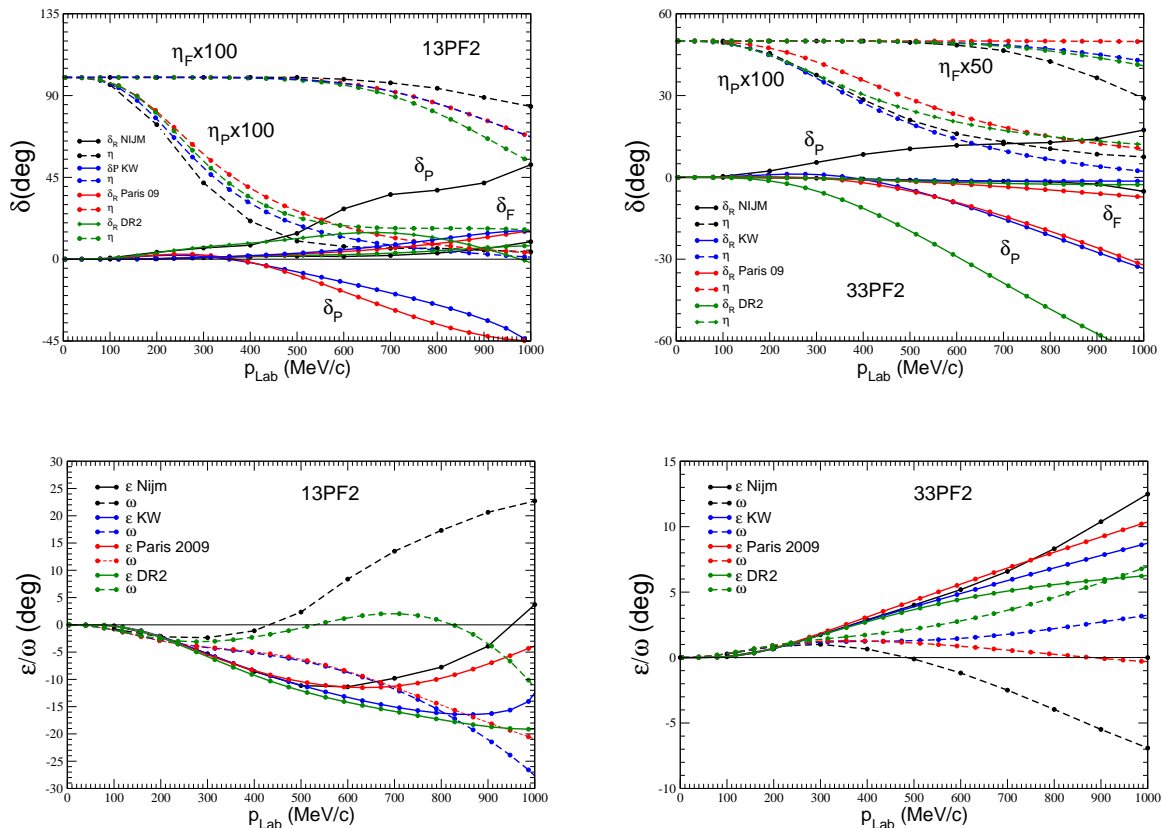


**Fig. 9**  ${}^3\text{PF}_2$   $\bar{N}N$  bare phase shifts and inelasticities (upper panel) and mixing parameters (lower panel), as functions of the  $\bar{N}$  laboratory momenta.

Furthermore the - very small - inelasticity parameter  $\eta$  enters quadratically as in the annihilation cross sections (16) from where it should, in principle, be extracted. However, the possibility to extract from the data analysis a significant signal of the order of  $10^{-4}$  seems unrealistic. This is specially true in an observable largely dominated by  ${}^3\text{SD}_1$  and  ${}^3\text{PF}_2$  partial waves, at the considered values of  $p_{\text{Lab}} \approx 600$  MeV/c.

On another hand to generate a model exhibiting zeros of the S-matrix, practically at the same point of the real axis, in different partial waves appears to be extremely artificial.

For all these reasons, we believe that the possibility for a PWA, to move from one solution to another one in the vicinity of the minima of the inelasticity parameter, should not be disregarded.

One can thus conjecture that the phase shifts in the vicinity of the  $\delta_I$  peak, could, in fact, be continued without exhibiting any resonant-like behaviour, as it happens in all the discussed models, and as it was considered in Refs. [42,43] for the  ${}^1\text{S}_0$  state. This would

not eliminate all the before mentioned inconsistencies among the  $\bar{N}N$  optical models but will greatly simplify the analysis in these two partial waves.

While the above presentation of the phase shifts has some interest for a global understanding of the interaction, it is not very useful for a detailed comparison of the models at low energy. Apart from the poor determination of the phase shifts themselves, the  $L > 0$  states have a low-energy behaviour like  $\delta(q) \approx -a_L q^{2L}$  which hides their contribution in this energy region.

One can remove the "centrifugal term" by redefining the reduced phase shifts  $\bar{\delta} = \delta/q^{2L}$ , as it was done in [41], but we believe it is more instructive to compare the effective range functions  $Z_\alpha$  and their dependence on the center of mass momenta  $q$  for the different partial waves. This will be done in the following section.

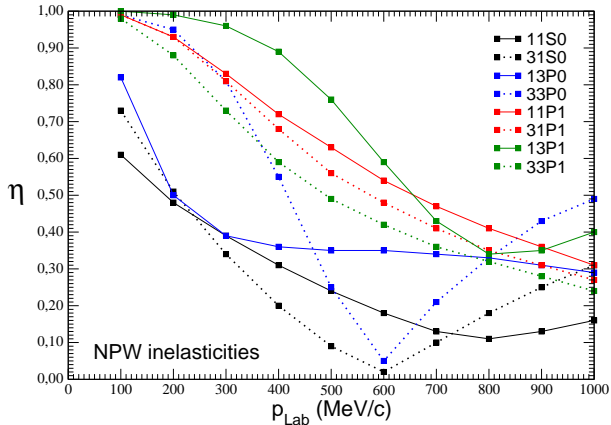


**Fig. 10** Inelasticity parameter  $\eta$  in the NPW as function of the  $\bar{N}$  laboratory momenta.

### 3.2 The Effective range functions and low energy parameters

For the tensor decoupled states the effective range functions  $Z_\alpha$  take the form

$$Z_\alpha(q^2) = q^{2L+1} \cot \delta_\alpha = -\frac{1}{a_\alpha} + \frac{1}{2}r_\alpha q^2 + o(q^4) \quad (20)$$

It is interesting to plot this quantity as function of  $q^2$ , for it easily allows to determine the validity region of the effective range expansion (ERE), explicated in eq. (20), and given by the linearity domain near the origin.

Notice that the value at the origin  $Z(0)$

$$Z(0) = Z(0)_R + i Z(0)_I = \frac{-a_R + ia_I}{|a|^2} \quad (21)$$

is related to the scattering length as

$$a_R = -|a|^2 Z(0)_R = -\frac{Z(0)_R}{|Z(0)|^2}$$

$$a_I = |a|^2 Z(0)_I = \frac{Z(0)_I}{|Z(0)|^2} \quad (22)$$

In particular one has imperatively  $Z(0)_I < 0$ .

In what follows we will display  $Z_\alpha(q^2)$  for all the considered PW. First (left panel), in the full energy domain  $q^2 \in [0, 3] \text{ fm}^{-2}$ , which correspond to  $p_{Lab} \leq 700 \text{ MeV/c}$ . Next (right panel of the same figure), presents a zoom in the low energy region  $q^2 \in [0, 0.2] \text{ fm}^{-2}$  ( $p_{Lab} \leq 180 \text{ MeV/c}$ ) to better exhibit the linearity domain and determine the low energy parameters ( $a_\alpha, r_\alpha$ ), abusively denoted scattering "length" and effective "range". The scattering length is given by the  $Z(0)$  value, following eq. (21), and the effective range from (twice) the slope at the origin.

The colour and model conventions are the same as those used for the phase shifts: real part of  $Z$  is plotted by solid lines and the imaginary part by dashed lines.

The extracted LEP values are collected in Tables 2 and 3 for the considered models and PWs. The NPW results given in [7] were limited to  $p_{Lab} \leq 100 \text{ MeV/c}$ . We have quadratically extrapolated their values at the origin by using the 3 lowest points. They are denoted by Nijm\* in Tables 2 and 3 and may have only an indicative value, in particular by comparing them to Julich results. Despite of this naive extrapolation, they all fulfil  $Z(0)_I < 0$ .

**The results for the  $^1S_0$  state** are displayed in Fig. 11. The upper panel correspond to  $T=0$  and the lower one to  $T=1$ .

The particular behaviour of Paris results is manifested, both in the real as well as the imaginary phase shifts in all the energy domain. One finds however a qualitative agreement among the other models including NPW.

As one can see from the right upper figures, the  $Z(q^2)$  dependence of the  $T=0$  state for the Paris potential is totally flat in the full domain. For the other models, the ERE is valid only at relatively low energy  $q^2 \leq 0.05 \text{ fm}^{-2}$ , i.e is  $p_{Lab} \approx 120 \text{ MeV/c}$ . Beyond this energy, the  $q^4$  terms neglected in (20) become relevant, and any linear extrapolation in  $q^2$  would lead to wrong results.

The  $Z(q^2)$  dependence for the  $T=1$  state (lower panels) is fairly smooth, with no visible trace of the NPW resonant-like behaviour manifested in the corresponding phase shift (right panel of Fig 2) at  $p_{Lab} \approx 600 \text{ MeV/c}$  ( $q^2 \approx 2.25 \text{ fm}^{-2}$ ). The differences among the models are much smaller than for  $T=0$  (except for Paris potential) and lead to scattering length values which are positive and consistent to each other within 15 % (see Table 2).

**The effective range functions for the P-waves are displayed in Figures 12 to 14.** In this representation the low-energy part is magnified with respect to the phase shifts and one can see that, as it was the case for S-waves, sizeable differences among the models themselves and with respect to the NPWA emerge.

**Figure 12 shows  $Z(q)$  for the  $^1P_1$  state.** For  $T=0$ , the results of the real part (left upper panel) have a similar qualitative behaviour: monotonously increasing from the origin until a maximum value and decreasing with a zero crossing towards negative region. However, although the Paris, DR and KW models are close to each other up to  $q^2=0.5 \text{ fm}^{-2}$  ( $p_{Lab} \approx 300 \text{ MeV/c}$ ),

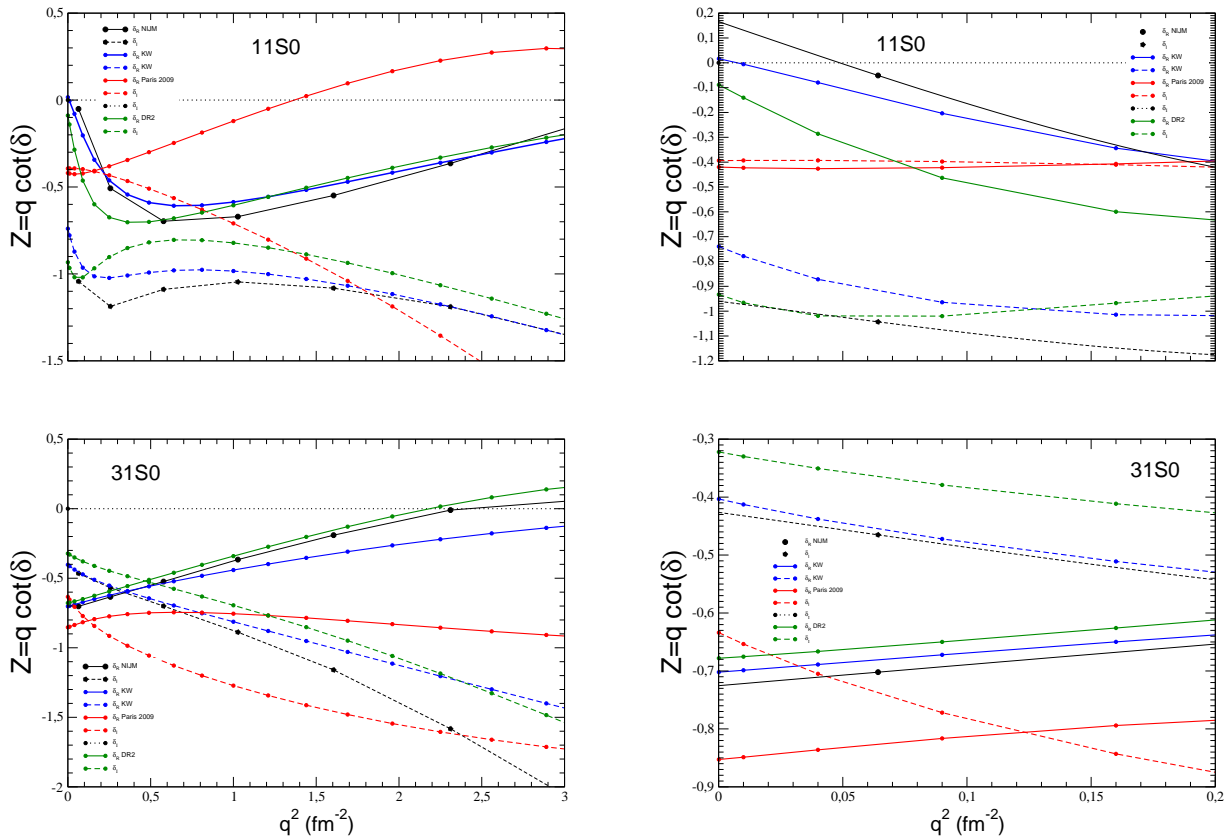


**Fig. 11** Effective range function (20) for the  $\bar{N}N$   $^1S_0$  states as function of the center of mass momentum squared (in  $\text{fm}^{-2}$ ). Upper figures correspond to  $T=0$  and the lower ones to  $T=1$ . In both cases, the right figure is a zoom of the left one, restricted to the low energy domain  $q^2 \in [0, 0.2] \text{ fm}^{-2}$  ( $p_{Lab} \leq 180 \text{ MeV}/c$ ), where the ERE of (20) is manifested by the linear behaviour near the origin.

they differ significantly at high energy, specially with respect the NPW results.

For  $T=1$  (lower panels) the dispersion is even larger and starts at low energy. Notice that the DR2 model displays a fast increasing near the origin which suggest a near-threshold resonant state. It manifests also in the lower right panel with an ERE breaking below  $q^2 = 0.05 \text{ fm}^{-2}$ .

Despite these differences in the model predictions, it is worth noticing the remarkable stability of the real part of the scattering volumes for both isospin states. They remain all between a 15% difference band, as one can see in Table 3. A possible reason of this stability will be discussed at the end of the section. The essential differences between models are in fact given by their absorptive parts. These could, in principle, be settled by additional measurements of the full fine structure in antiprotonic atoms. Unfortunately this measurement still waits for its turn [50].

**The results for  $^3P_0$  wave are shown in Figure 13.** Again, for  $T=0$  the real phase shifts a general qualitative agreement is observed among DR, KW and Paris models in a more extended energy region, with a departure from NPW already at  $q = 0$ . The validity of the ERE expansion (upper right panel) extends up to  $q^2 = 0.2$ . Except for the Jülich model, the corresponding scattering volumes have a large real part, attributed in [41] to the existence of a near-threshold bound or resonant state, and are in a very close agreement ( $<2\%$ ).

For  $T=1$ , the NPW resonance-like structure displayed in Fig 5 at  $p_{Lab} \approx 600 \text{ MeV}/c$  leaves no trace in the effective range function  $Z$ . However a similar structure – absent at the level of phase shifts – is seen in  $Z$  at  $q^2 = 0.5 \text{ fm}^{-2}$ , breaking any possible agreement with the other optical models. The corresponding scattering lengths (real part) remain close within 15% and the imaginary part is very small.

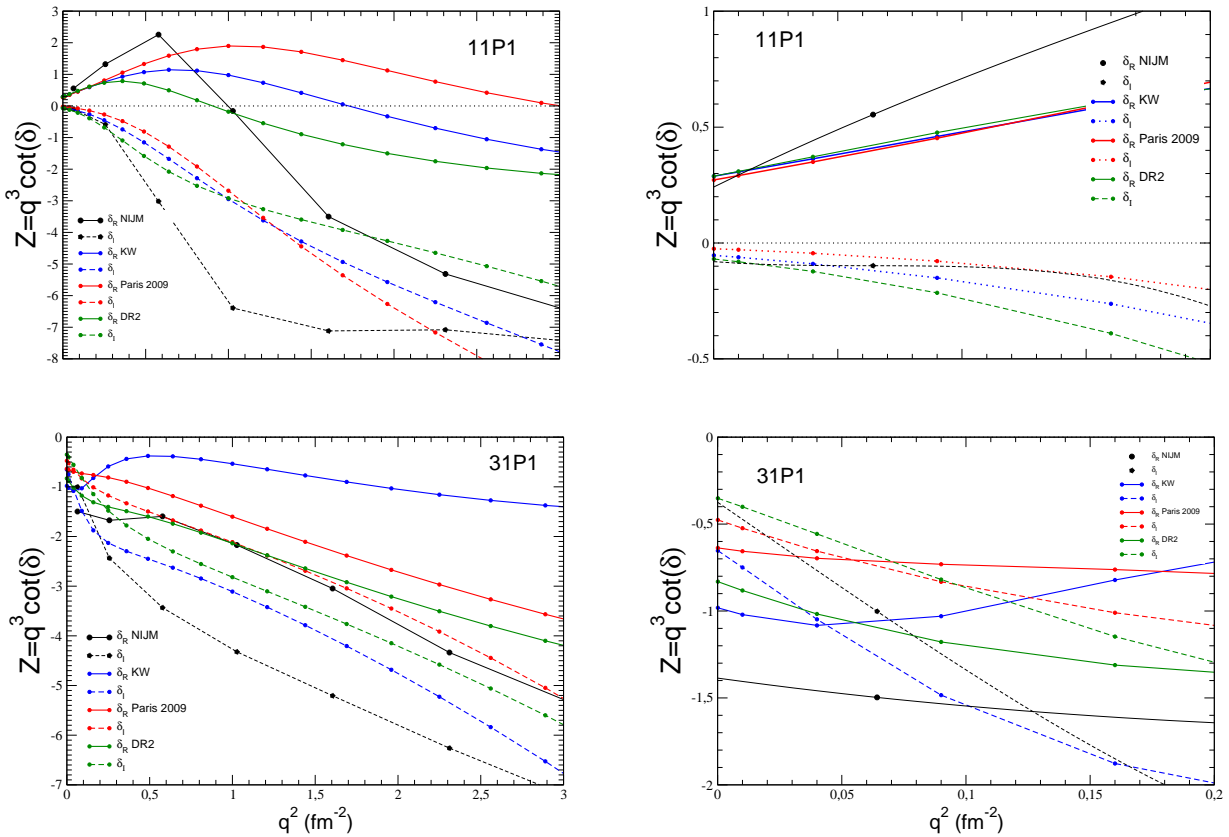


**Fig. 12** Effective range function (20) for the  $\bar{N}N$   $^1P_1$  state as function of the center of mass momentum squared (in  $\text{fm}^{-2}$ ), with the same convention as in figure 11.

The  $^3P_1$  effective range functions  $Z(q^2)$  are displayed in Figure 14 for both isospin channels. The  $T=0$  state (upper panel) is the most stable partial wave, for the real as well as for the imaginary part. This is probably due to the  $^{13}P_1$  potential, repulsive in all the models, which also explains the small imaginary part

The quantitative disagreements start only above  $q^2 \approx 1 \text{ fm}^{-2}$  ( $p_{Lab} \approx 400 \text{ MeV}/c$ ) and increase with the energy. The ERE (right panel) works perfectly in all the domain and the LEPs (both  $a_1$  and  $r_1$ ) are in close agreement, with an almost vanishing imaginary part.

For  $T=1$ , the main difference comes Paris 2009, which displays a different qualitative behaviour in all the energy domain, including the LEPs. As mentioned, this particular feature is due to a quasi-bound state generated in this model at  $E=-3.6-i12.4 \text{ MeV}$ . The other optical models are in quite a good agreement.

The low energy parameters ( $a_L$  and  $r_L$ ) of the examined partial waves are collected in Table 2 for S-waves

and Table 3 for P-waves. In view of these results some general remarks can be drawn. They are in order:

1. Despite the huge differences in the phase shifts described in this and the previous sections, there is a remarkable stability in the "qualitative" zero-energy predictions, mainly the scattering lengths and volumes. We mean by that their "repulsive" or "attractive character", more precisely the sign of their real part, the almost vanishing imaginary part of  $^{13}P_1$  and  $^{33}P_0$  states, or the relatively small values of the  $^3PF_2$ . This is specially true if one take into account that none of these models has been adjusted in order to reproduce the zero energy protonium results and that the potential themselves are very different. For the S-waves, only the  $^{11}S_0$  result of Paris and DR2 potentials have different sign. For the P-waves, the only exception in this general qualitative agreement is the  $^3P_1$  state, again due to Paris potential which has a different sign. As we have already noticed, the reason for this difference

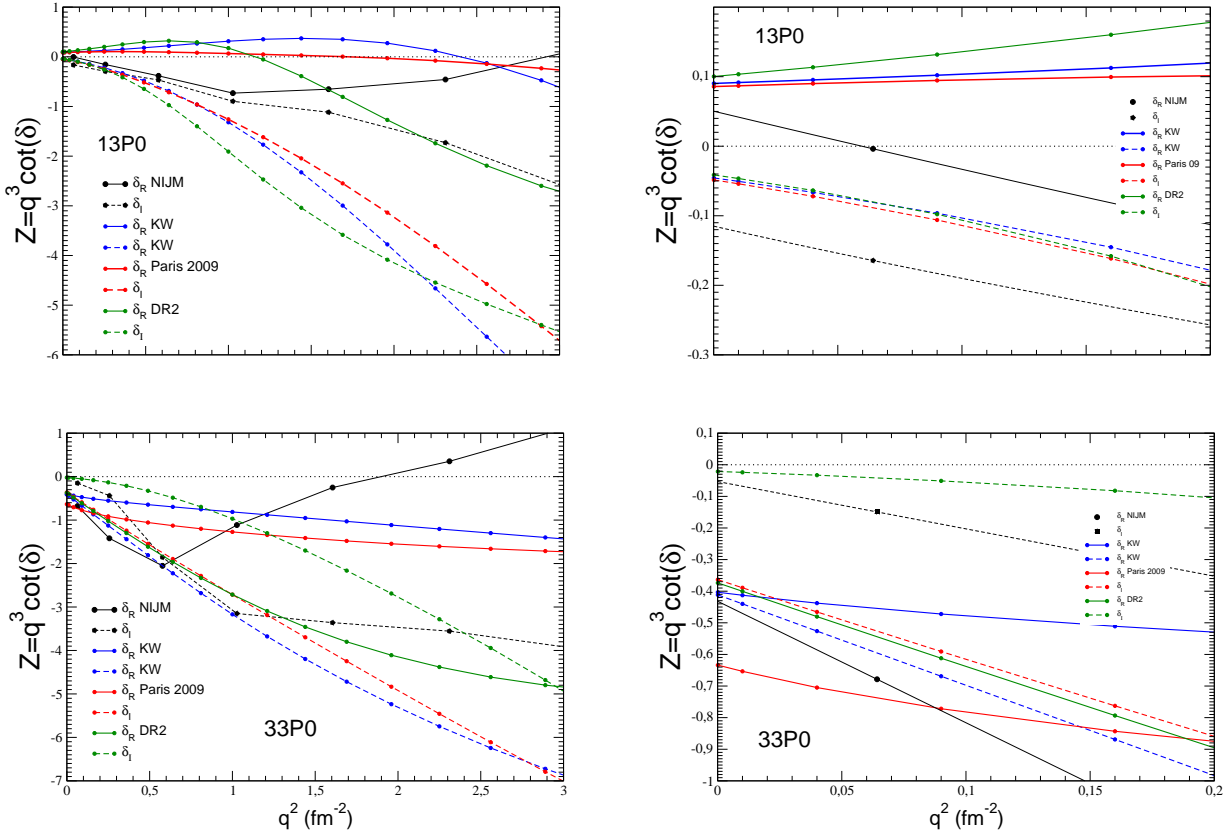


**Fig. 13** Effective range function (20) for the  $\bar{N}N$   ${}^3P_0$  state as function of the center of mass momentum squared (in  $\text{fm}^{-2}$ ) and the same conventions as in figure 11.

is in both cases related to a near threshold quasi-bound state in the corresponding PW.

Furthermore, in most of the sates, this agreement is not only qualitative but there is a reasonable quantitative agreement (between 10-20% with respect their averaged) in the numerical values, except in some particular states and models that we will detail below.

2. A possible explanation for this astonishing stability in the real parts could be the one-pion exchange dominance, as it was suggested by Ericson and Weise for the NN case (see Sect 3.8 of Ref. [45]). Indeed, for a tensor uncoupled state, the integral form for the scattering "length" can be written as

$$a_L = \lim_{q \rightarrow 0} \frac{1}{q^{2L+2}} \int_0^\infty dr \hat{j}_L(qr) v(r) u_L(r) \quad (23)$$

where  $v = \frac{m}{\hbar^2} V$  is the corresponding potential,  $\hat{j}_L$  the reduce regular spherical Bessel and  $u_L$  the reduced radial solution that behaves asymptotically as

$$u_L(r) = \hat{j}_L(qr) + \tan \delta_L \hat{n}_L(qr)$$

According to these authors, a good approximation of  $a_L$  (for  $L > 0$ ) is provided by the Born approximation of the one-pion potential tail  $v_\pi$ , that is:

$$a_L^B(\pi) = \lim_{q \rightarrow 0} \frac{1}{q^{2L+2}} \int_0^\infty dr |\hat{j}_L(r)|^2 v_\pi(r) \quad (24)$$

By inserting the one-pion potential

$$V_\pi(x) = c_\pi [\sigma \cdot \sigma + S_{12} \chi_T(x)] Y(x) \tau \cdot \tau \quad (25)$$

with  $x = \frac{m_\pi r}{\hbar}$ ,

$$c_\pi = \frac{m_\pi g^2}{3} \frac{1}{4\pi} \left( \frac{m_\pi}{2M} \right)^2,$$

$$Y(x) = \frac{e^{-x}}{x},$$

and

$$\chi_T(x) = 1 + \frac{3}{x} + \frac{3}{x^2}$$

into eq. (24) one gets:

$$a_L^B(\pi) = \frac{c_\pi}{(2L+1)!!^2} \left( \frac{M}{\hbar^2} \right) \left( \frac{\hbar}{m_\pi} \right)^{2L+3} (\tau \cdot \tau)$$



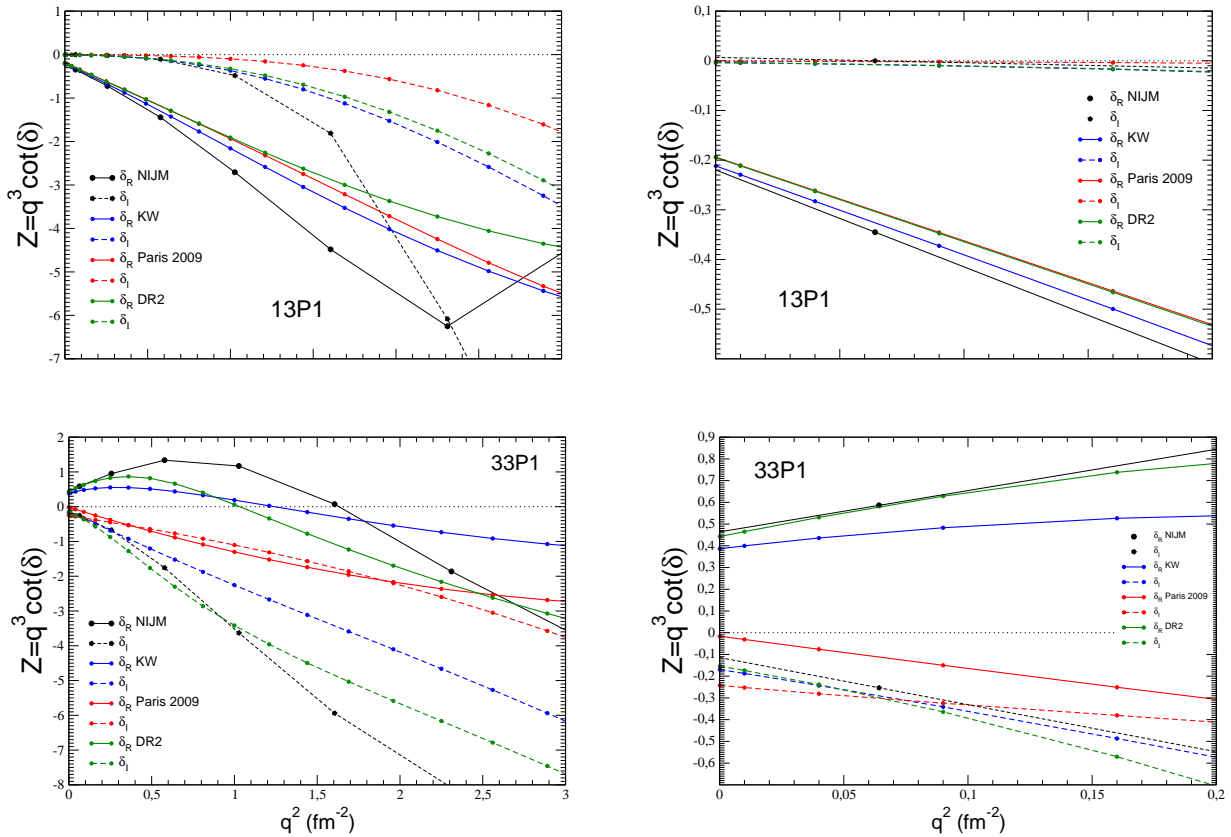


**Fig. 14** Effective range function (20) for the  $\bar{N}N$  3P1 state as function of the center of mass momentum squared (in  $\text{fm}^{-2}$ ), with the same convention as in figure 11.

$$\left\{ (\sigma \cdot \sigma)(2L+1)! + S_{12} \left[ (2L+1)! + 3[(2L)! + (2L-1)!] \right] \right\}$$

The first remark about the later expression is the "τ·τ rule", i.e the fact that the ratio of the scattering lengths of two isospin components of the same PW is given by the value of τ·τ operator: τ·τ=-3 for T=0 and τ·τ=1 for T=1. Indeed the real part of the scattering volumes displayed in Table 3 (uncoupled states) roughly fulfil this requirement. There are two exceptions: the results of Nijmegen-Jülich  $^3P_0$  (in relative sizes) and the Paris  $^3P_1$  (in relative sizes and signs).

By using the numerical values  $m_\pi=138.039$  MeV,  $M=938.9183$  MeV (averaged pion and N masses) and  $g^2/4\pi=14.4$ , one obtains for the  $\bar{N}N$  states the results displayed in Table 4. The  $^3P_2$  results is decoupled from the  $^3F_2$  tensor partner. With the recommended NPW  $\pi NN$  coupling constant  $g^2/4\pi=13.9$ , a reduction factor 0.965 must be used.

For  $^1P_1$  state, the Born pion values are close (15%) to the full results from Table 3, except for KW where the difference is twice larger.

For  $^3P_0$ , the differences are of the same order. Only the  $^{13}P_0$  Jülich result shows a large discrepancy in the τ·τ rule.

For  $^3P_1$ , the agreement is even better, except for the instructive Paris result which differs substantially. Indeed the "one-pion exchange dominance" is based on the assumption that the scattering solution  $u_L$  is close to the free wave  $\hat{j}_L$  in the dominant part of the integral (23). In case of the existence of a bound state, as in the Paris model,  $u_L$  has a node and change its sign with respect to the free solution. For  $^3PF_2$ , the Born results from eq. (24) cannot directly be applied since they were established for tensor uncoupled states. However for the single  $^3P_2$  state they predict a vanishing  $\text{Re}(a)$  and the small value of the full results from Table 3 could be a trace of this compensation.

To close this remark, we would like to mention that while the "one-pion exchange dominance" is justified in the NN case, where it was established, it has an uncertain applicability in the  $\bar{N}N$  physics.

	$a_0$	$r_0$	$a_0$	$r_0$
T=0	$^{11}\text{S}_0$		$^{13}\text{SD}_1$	
Nijm*	-0.17 -1.01i	-6.9-2.9 i	–	–
Jülich	-0.21 -1.23i	–	1.42-0.88i	–
Paris 09	1.27 -1.18i	-0.53+0.14i	1.20-0.80i	–
KW	-0.03 -1.35i	-4.7-7.9i	1.23-0.77i	–
DR2	0.10 -1.07i	-11-6.2i	1.28-0.78i	–
T=1	$^{31}\text{S}_0$		$^{33}\text{SD}_1$	
Nijm*	1.02 -0.60i	0.7-1.2i	–	–
Jülich	1.05 -0.58i	–	0.44-0.96i	–
Paris 09	0.76 -0.56i	0.9-3.9i	0.61-0.44i	–
KW	1.07 -0.62i	0.7-1.9i	0.78-0.80i	–
DR2	1.20 -0.57i	0.6-1.6i	0.89-0.71i	–

**Table 2** S-wave  $\bar{N}N$  low energy parameters (in fm) for the considered optical models: Jülich results are taken from Tab 3 of Ref. [12], KW and DR2 from [18], Paris 2009 have been recomputed and are in agreement with [44]. The values of Nijmegen are obtained by extrapolating the phase shifts from Figures 2 and 3.

Apart from disregarding the annihilation physics, this approach will fail in presence of one or several bound or resonant states, as it is the case in most of  $V_{\bar{N}N}$  models. We have seen an illustrative example in the  $^{33}\text{P}_1$  case with Paris results having different sign. However the same breakdown of the "one-pion exchange dominance" can happen if there are two bound states, although keeping the same sign. This can be the case of the  $^{13}\text{P}_1$  state with KW or the  $^{13}\text{P}_0$  with Jülich where the  $\tau \cdot \tau$ -rule is badly violated.

3. The imaginary part of S-waves is also remarkably stable within quite narrow limits  $\text{Im}[a(^{11}\text{S}_0)]=1.18 \pm 0.17$  fm,  $\text{Im}[a(^{31}\text{S}_0)]=0.60 \pm 0.03$  fm and  $\text{Im}[a(^{13}\text{SD}_1)]=0.82 \pm 0.05$  fm. Only the  $^{33}\text{SD}_1$  state presents some dispersion essentially due to Paris result, with  $\text{Im}[a(^{33}\text{SD}_1)]=0.73 \pm 0.30$  fm.

The imaginary part of P-waves is much less stable, although some common features are shared like the small values for the  $^{13}\text{P}_1$ , due to its repulsive character.

4. Of particular interest is the  $^{13}\text{P}_0$  state, with a very large real part  $\sim 9$  fm<sup>3</sup> shared by DR, KW and Paris models (Jülich results are 3 times smaller), and confirmed by protonium data. This large and negative value was attributed in [41] to the existence of a near-threshold state. However it finds also a "natural" explanation in terms of the "pion dominance" in Table 4, which predicts  $\text{Re}(a)=-9.3$  fm<sup>3</sup>. This, at first glance, puzzling situation can be reconciled if one takes into account the result of Ref. [46], according to which, in the chiral limit ( $m_\pi=0$ ), the NN  $^3\text{P}_0$  state (so T=1) has a zero energy virtual state, with a diverging scattering volume. The existence

of such a NN bound state, as well as some related consequences in nuclear matter, is prevented by the short range NN repulsion, which is however absent in the  $\bar{N}N$  case and leave open such a possibility.

5. The most stable states are those with a repulsive potential. These are the  $^{13}\text{P}_1$  and  $^{33}\text{P}_0$ . They have in common a small imaginary part both in  $a_1$  and  $r_1$  since they are little sensitive to annihilation dynamics. For  $^{13}\text{P}_1$ , all models agree with a real part of  $4.9 \pm 0.3$  fm<sup>3</sup> and an imaginary part smaller than 0.1 fm<sup>3</sup>. For  $^{33}\text{P}_0$ , they all agree with a real scattering volume  $2.5 \pm 0.25$  fm<sup>3</sup> and a small imaginary part  $\sim 0.1$  fm<sup>3</sup>. The Paris potential is a particular case:  $V_{33P_1}$  is attractive with a quasi-bound state previously discussed. However  $V_{13P_1}$  is even more attractive than the former but has a positive  $\text{Re}[a_{13P_1}]$  as for the repulsive models. This suggest the existence of a second bound state for the  $^{13}\text{P}_1$  state which plays the role of an effective repulsion.
6. Concerning the effective range values  $r_L$  there is no any trace of stability in the model predictions, which translate the fact that beyond the zero energy region the examined  $\bar{N}N$  optical models display larger differences.

### 3.3 Hydrogen atoms

The measurement of level shifts and widths in Hydrogen atoms is an alternative way to access the  $\bar{p}p$  scattering lengths and volumes. A formula derived by Trueman [47] finds a connection between the protonium complex level shifts and the Coulomb corrected  $\bar{p}p$  scattering lengths. In the case of antiprotonic hydrogen, due to large Bohr radius ( $B \approx 57$  fm), this relation is essentially linear [18].

The  $\bar{p}p$  scattering lengths are obtained by coupling both T components by Coulomb and  $\Delta m$  corrections. One obtains however a reasonable approximation, denoted  $a_{\bar{N}N}$  to distinguish it from the exact value  $a_{\bar{p}p}$ , by neglecting this coupling and isospin-averaging the results of Tables 2 and 3, i.e:

$$2 a_{\bar{N}N} = a_{T=0} + a_{T=1} \quad (26)$$

Table 5 shows the comparison between the computed values  $-a_{\bar{N}N}$  and  $a_{\bar{p}p}$  – and those extracted from the atomic measurements [48] via the Trueman relation. Notice that the inclusion of Coulomb and  $\Delta m$  can represent up to a  $\approx 30\%$  difference between  $a_{\bar{N}N}$  and  $a_{\bar{p}p}$  values.

For S-waves the discrepancies existing in Table 2 within the different models, mainly concerning the  $^{11}\text{S}_0$

	$a_1$	$r_1$	$a_1$	$r_1$	$a_1$	$r_1$	$a_1$	$r_1$
T=0	$^{11}\text{P}_1$		$^{13}\text{P}_0$		$^{13}\text{P}_1$		$^3\text{PF}_2$	
Nijm*	-3.34-1.22i	9.3-1.2i	-3.06-7.23i	-1.7-1.5i	4.36-0.00i	-3.5-0.0i	-	-
Jülich	-2.87-0.36i	-	-2.83-7.82i	-	4.61-0.05i	-	-0.74-1.13i	-
Paris 09	-3.62-0.34i	3.8-0.8i	-8.78-4.99i	0.23-1.1i	5.12-0.02i	-3.4-0.02	-0.49-0.87i	-
KW	-3.36-0.62i	3.7-1.6i	-8.83-4.45i	0.25-0.97i	4.73-0.08i	-3.5-0.1i	-0.46-1.09i	-
DR2	-3.28-0.78i	4.2-2.3i	-8.53-3.50i	0.63-1.0i	5.14-0.09i	-3.4-0.1i	-0.59-0.85i	-
T=1	$^{31}\text{P}_1$		$^{33}\text{P}_0$		$^{33}\text{P}_1$		$^3\text{PF}_2$	
Nijm*	0.66-0.18i	3.3-20i	2.33-0.92i	-10-0.7i	-2.02-0.70i	4.7-2.8i	-	-
Jülich	0.80-0.34i	-	2.18-0.19i	-	-2.04-0.55i	-	-0.48-0.34i	-
Paris 09	1.00-0.77i	-3.7-9.8i	2.74-0.00i	-5.2-0.01i	0.28-4.11i	-3.0-2.0i	-0.13-0.21i	-
KW	0.71-0.47i	-8.3-21i	2.43-0.11i	-5.8-0.43i	-2.17-0.95i	2.7-3.5i	-0.30-0.45i	-
DR2	1.02-0.43i	-11-10i	2.67-0.15i	-5.4-0.53i	-2.02-0.70i	4.6-3.9i	-0.04-0.53i	-

**Table 3** P waves  $\bar{N}N$  low energy parameters (in  $\text{fm}^3$ ) for the considered optical models: Jülich results are taken from Tab 3 of Ref. [12], KW and DR2 from [18], Paris 2009 have been recomputed and are in agreement with [44]. The values of Nijmegen are obtained by extrapolating the phase shifts from Figures 2 and 3.

	$\sigma \cdot \sigma$	$\tau \cdot \tau$	$S_{12}$	$\text{Re}[a_L]$
$^{11}\text{P}_1$	-3	-3	0	-3.09
$^{31}\text{P}_1$	-3	1	0	1.03
$^{13}\text{P}_0$	1	-3	-4	-9.27
$^{33}\text{P}_0$	1	1	-4	3.09
$^{13}\text{P}_1$	1	-3	2	6.18
$^{33}\text{P}_1$	1	1	2	-2.06
$^{13}\text{P}_2$	1	-3	-2/5	0
$^{33}\text{P}_2$	1	1	-2/5	0

**Table 4**  $\bar{N}N$  scattering volumes ( $\text{fm}^3$ ) as predicted by the pion dominance from [45]

state, are smeared out in the T and S-averaged value, which is found to be in a nice agreement among them and with the experimental value. A remarkably good agreement is also observed in the, non trivial,  $^3\text{SD}_1$  state. The major problem to improve the situation for S-waves is the  $^{11}\text{S}_0$  near-threshold quasi-bound state, present in Paris and probably DR2 models but absent in KW and Jülich ones. It results into a negative value of the corresponding scattering length and that generates a factor 2 in the real parts.

For P-waves, little is known experimentally. The measurement of the isolated  $^3\text{P}_0$   $\bar{p}p$  level shift [50] seems to confirm the large value of the  $^{13}\text{P}_0$  scattering volume displayed in Table 3, predicted by Paris, KW and DR2 models. In fact the large value of  $\text{Re}[^{13}\text{P}_0] \approx -9 \text{ fm}^3$  that they predict, and that is averaged with a positive  $\text{Re}[^{33}\text{P}_0] \approx 2.5 \text{ fm}^3$ , is still underestimated for reproducing the experimental result. One would rather need  $\text{Re}[^{13}\text{P}_0] \approx -13 \text{ fm}^3$ . This is clearly in tension with the Jülich prediction which is one order of magnitude smaller than the other models and the experimental value.

Since the large values of  $\text{Re}[a_{13\text{P}_0}]$  are predicted by the "pion dominance" described in the previous section, one could find an explanation of this disagreement in the particular form of the one-pion potential (eq. 2.1 of [12]), which includes a non-local relativistic correction and results into a smaller effective  $\pi NN$  coupling constant.

As polarisation experiments are missing, the atoms offer a unique possibility to study the spin structure of interactions. Again, there are sizeable differences between the models. Unfortunately these happen also in the absorptive parts which are vital for the PUMA experiment. These should be resolved on the side of theory and more important on the side of experiments. The priority, we believe, should be given to the full resolution of the atomic fine structure in Hydrogen and Deuterium. In particular the  $2P$  state in Hydrogen displays a clear  $^3\text{P}_0$  state, indicated in Table 5 and three other states lumped together and difficult to resolve. See Ref [50] for a dedicated review. An improvement of this resolution would be extremely helpful to eliminate the model differences in the partial waves.

## 4 Conclusion

We have compared the strong  $\bar{N}N$  phase shifts obtained in the Nijmegen Partial Wave Analysis [7], used to construct the chiral EFT Jülich optical potential at N3LO [12], with some of the currently used  $\bar{N}N$  optical models in configuration space: Dover-Richard (DR2) [20, 21], Kohno-Weise [22] and Paris (updated version from 2009) [19]. For all these models we have computed the strong phase shifts and extracted the low energy parameters (scattering lengths and effective ranges). The corresponding potentials are included in the Appendix. This comparison is limited to the S and P waves.

state		Exp	Paris 2009	Jülich	KW	DR2
$^1S_0$	$\bar{N}N$		1.02 - i 0.87	0.42 - i 0.91	0.52 - i 0.99	0.65 - i 0.82
	$\bar{p}p$	0.493(92) - i 0.732(146)	0.92 - i 0.67	0.50 - i 0.71	0.57 - i 0.77	0.68 - i 0.64
$^3SD_1$	$\bar{N}N$		0.91 - i 0.62	0.93 - i 0.92	1.01 - i 0.79	1.09 - i 0.75
	$\bar{p}p$	0.933(45) - i 0.604(51)	0.82 - i 0.50	0.90 - i 0.74	0.92 - i 0.63	0.98 - i 0.59
S-averaged	$\bar{N}N$		0.94 - i 0.68	0.80 - i 0.92	0.89 - i 0.84	0.98 - i 0.77
	$\bar{p}p$	0.823(57) - i 0.636(75)	0.85 - i 0.54	0.80 - i 0.74	0.83 - i 0.67	0.90 - i 0.60
$^3P_0$	$\bar{N}N$		-3.02 - i 2.50	-0.32 - i 4.01	-3.20 - i 2.28	-2.93 - i 1.83
	$\bar{p}p$	-5.68(123) - i 2.45 (49)	-2.74 - i 2.46	-0.32 - i 3.85	-2.81 - i 1.99	-2.53 - i 1.62

**Table 5** Isospin averaged ( $a_{\bar{N}N}$ ) and  $\bar{p}p$  scattering lengths are compared with those obtained from hydrogen atom level shifts and widths, in fm for S and fm<sup>3</sup> for P states. The  $\bar{p}p$  values including Coulomb and  $\Delta m$  corrections are taken from [18] for DR2 and KW, from [19] for Paris and from [12] for Jülich model. The statistical averaged value for S-wave is defined as ( $^1S_0 + 3\ ^3S_1$ )/4 and is given with averaged errors.

In spite of providing very close elastic, annihilation and charge-exchange integrated cross sections (Figure 1), these models are not phase-equivalent: large and systematic differences have been observed in almost all the partial waves, among them and with respect to the NPWA.

In the low energy region one observes some stability in the scattering lengths and volumes (Tables 2 and 3), in particular the "repulsive" or "attractive" character, i.e. the sign of  $\text{Re}[a_L]$ , which is respected by all models in almost all partial waves. For P-waves this stability could be related to the "one-pion exchange dominance", that is scattering volumes roughly determined by the pion Born term. It is however also manifested in S-waves, like the surprising stability of the low energy parameters of the tensor coupled  $^3SD_1$  state. Exceptions are the  $^1S_0$  and  $^3P_1$  partial waves, due to the presence of a nearthreshold quasi-bound state in DR2 and Paris, and the  $^3P_0$  result of Jülich model which underestimates the protonium experimental measurements. Despite these isolated differences, the isospin- and spin-averaged values for S-wave are in close agreement among the models themselves as well as with the measured quantities (Table 5). The later concern mainly the  $\bar{p}p$  measurements and so are unable to disentangle a selected isospin component.

The differences worsen when increasing the energy, as it is already manifested with the dispersion in the effective range values and more explicitly in the phase-shifts (Figures 2, 3, 4, 5, 8 and 9) and zoomed in the corresponding effective range functions. These increasing differences cannot be explained by the relativistic kinematics implemented in the Nijmegen Partial Waves Analysis, relating  $p_{Lab}$  to the center of mass momentum, or in the Jülich relativistic dynamical equation.

Our main conclusion in this work is that if the Nijmegen Partial waves analysis must be considered as a reference, as it was the case for the Jülich model [12], none of the examined optical potentials is com-

patible with these results and require quite a severe adjustment. This could be easily achieved if one limits to  $p_{Lab} \leq 400$  MeV/c, the main obstacle lies in the position of the near-threshold quasi-bound states.

On the other hand, we have pointed out some anomalous behaviours of the Nijmegen Partial Waves Analysis, also reported into the Jülich potential. They manifest as a resonant-like structures of the phase shifts in the  $^3S_0$  and  $^3P_0$  states which takes place at the same – relatively high – energy and which are difficult to interpret as having a dynamical origin, in particular in terms of resonant states. Furthermore they coincide with an almost zero of the S-matrix modulus (or inelasticity parameter) that can introduce a bias in the analysis or a spurious change from one solution to another. The existence of such structures in the phase shifts constitutes one of the major differences with respect to the examined optical models. It would be of the greatest interest to clarify this point or to better understand the underlying dynamics of these states. It would also be interesting to decrease the lowest energy value ( $p_{Lab}=100$  MeV/c) and eventually incorporate the protonium zero-energy data. This will not provide a magic solution of the observed discrepancies but will clearly facilitate the agreement of the models, in particular above  $p_{Lab} = 500$  MeV/c.

To have at our disposal a model-independent extraction of the strong  $\bar{N}N$  phase shifts, the non trivial part of the interaction, is of paramount importance to the field. In this respect it would be also suitable to have at our disposal an independent Partial Wave analysis, as it has been always the case in the simpler NN case.

All the examined models roughly reproduce the experimental  $\bar{p}p$  elastic, inelastic and charge-exchange total cross sections, including some differential cross sections. Unfortunately, these observables are computed at relatively high energy, result from a coherent and incoherent sum of many partial waves and hide the existing differences among them that have been evidenced here.

It would be of the highest interest to the community to develop, in parallel with more ambitious projects, an experimental program to measure the most complete set of  $\bar{N}N$  observables at energies  $p_{Lab} < 200$  MeV/c allowing to determine the main partial waves (S,P,D) that control the low energy structure calculations. In this energy domain we are not only faced to a bad "quality of data", but to a total lack of experimental results.

As far as we will not have at our disposal a reliable determination of the  $\bar{N}N$  strong phase shifts for the lowest partial waves, would they be limited to a restricted energy domain of few tens of MeV, any prediction concerning more complex systems, like those of interest in PUMA project, could be strongly model dependent.

## Acknowledgement

We are grateful for the support of the "Espace de Structure et de réactions Nucléaires Théorique" (ESNT, <https://e>) organizing a workshop and welcoming the visit of S. Wycech at CEA Saclay. This work was started during our visit to National Center for Nuclear Research in Warsaw. We thank the staff members of the theory group for their warm hospitality. We acknowledge the support of the CNRS/IN2P3 French-Polish COPIN agreement. We are thankful to Benoît Loiseau, Johann Haidenbauer and Ruprecht Machleidt for enlightening discussions and for providing us with their respective potentials.

## Appendix A: Potentials in configuration space

Although not being observable we believe it could be instructive to compare the potentials of the different models in a given partial wave. The Jülich model being in momentum space and non local is not included. The Paris potential is E-dependent and, except for the tensor-coupled states, we selected some positive and negative arbitrary values of  $E$ . For the NPWA, the inner part corresponds to the square well defining the boundary conditions at  $r=1.2$  fm. Beyond this value it is continued with the one- plus two-pion (N2LO) exchange potentials.

As one can see in the following figures, the  $\bar{N}N$  potentials exhibit quite dramatic differences, making even

difficult to assess whether the  $\bar{N}N$  interaction in a given PW is attractive or repulsive. This is in sharp contrast with the NN case.

### $^1S_0$

This partial wave is globally attractive in both isospins for all models, and much stronger than for the NN case, specially in T=1. However in the NPWA, there is no any need of short-range attraction in T=0. Paris potential presents two peculiar differences with respect to the other potentials: the strong short range repulsion, claimed to be imposed by phenomenology, and the repulsive peak at 1 fm, which cannot be justified in terms of pion- or omega-exchanges since they are shared by all models.

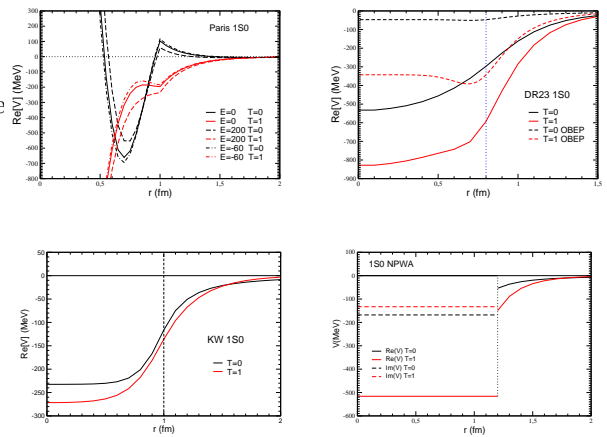


**Fig. 15** Real parts of  $^1S_0$  potentials for both isospins (T).

### $^3S_1$

The S-wave tensor-coupled state presents also some striking differences: the  $^{13}S_1$  potentials are strongly attractive wells, going from 500 MeV to several GeV depth, while the NPWA is limited to 130 MeV.  $V_{33S_1}$  is also deeply attractive in all models but turns to be slightly repulsive ( $\approx 50$  MeV) in the NPWA.

The  $^3S_1 \rightarrow ^3D_1$  transition potentials have in common that they are all very strong but they display also sizeable differences. Notice that in the DR and KW models the couplings don't vanish in the limit  $r \rightarrow 0$ , what spoils the usual  $r^{L+1}$  behaviour of the (reduced) radial wave functions.

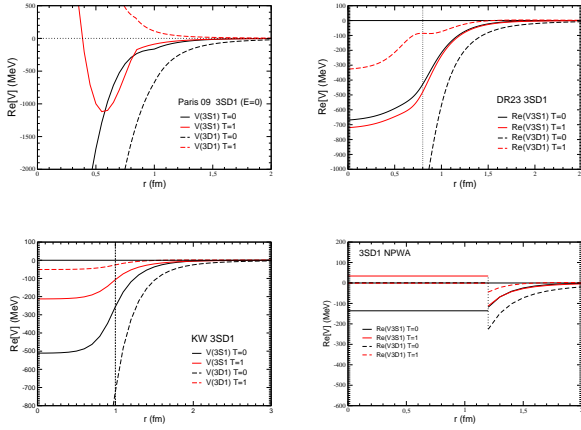


**Fig. 16** Real parts of  $^3S_1$  and  $^3D_1$  potentials for both isospins (T).

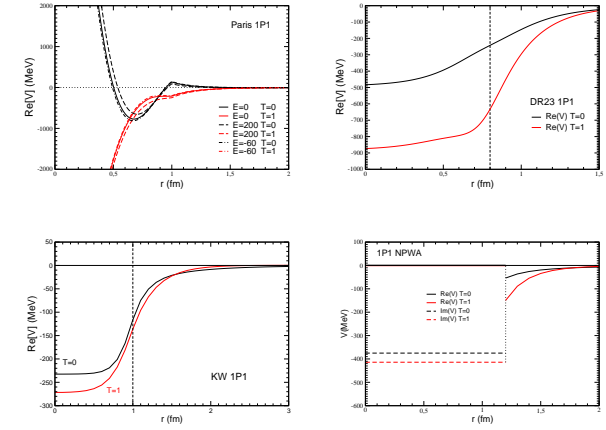


**Fig. 18** Real parts of  $^1P_1$  potentials for both isospins (T).

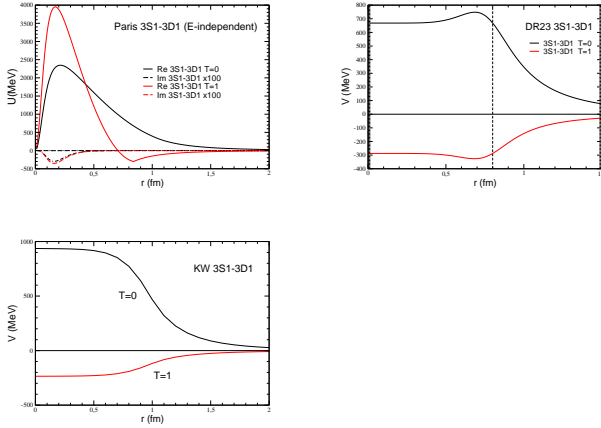


**Fig. 17**  $^3S_1 \rightarrow ^3D_1$  transition potentials for both isospins (T). They are real in DR and KW models.

$^1P_1$

Apart from the centrifugal barrier, this potential is very close to the  $^1S_0$  one in all models. Their difference is due to the attractive, Quadratic Spin-Orbit term ( $Q_{12}$ ), present in Paris and DR2 models but absent in KW. In the short range part of NPWA, the vanishing  $^{11}S_0$  potential displayed in Figure 15, vanishes also in the  $^{11}P_1$  state, indicating that there is no any  $Q_{12}$  contribution. However the strong (500 MeV) attraction present in the  $^3S_0$  state has now totally disappeared indicating rather an unexpected repulsion.

$^3P_0$

All models agree with a huge attraction in T=0 state,  $\sim 1$  GeV at  $r=1$  fm. The NPWA does not require such a large attraction and the fit is done with a potential depth of  $\approx 100$  MeV in the internal region, although matched with a pion potential of 350 MeV.

For T=1, and in view of the repulsive scattering lengths, there is also a general agreement in the repulsive character of the interaction, although the direct inspection of the potentials requires some caution.

In KW model, the  $^3P_0$  potential is repulsive everywhere, while DR2 has an attractive pocket below  $r=0.7$  fm which is fully compensated by the centrifugal term. Paris potential (at  $E=0$ ) has also a deep attractive pocket (-260 MeV) between  $r=0.5$  fm and  $r=0.7$  fm. It is almost totally compensated by the centrifugal barrier, but there remains a shallow attractive pocket (-35 MeV) between 0.56 and 0.63 fm. Under these dynamical conditions there is no room for developing a resonance, especially taking into account the repulsive E-dependent amplitude at positive energies. The examined models are, thus, globally repulsive.

However, the NPWA requires an overall attractive short range contribution of  $\approx 150$  MeV, though matched at  $r=1.2$  fm with a repulsive  $V_\pi$ .

$^3P_1$

This PW has repulsive scattering length in both isospin states. For T=0, KW, DR are indeed repulsive (once the centrifugal barrier is included) but NPW has an attractive pocket and Paris remains strongly attractive (2 GeV at  $r=0.5$  fm).

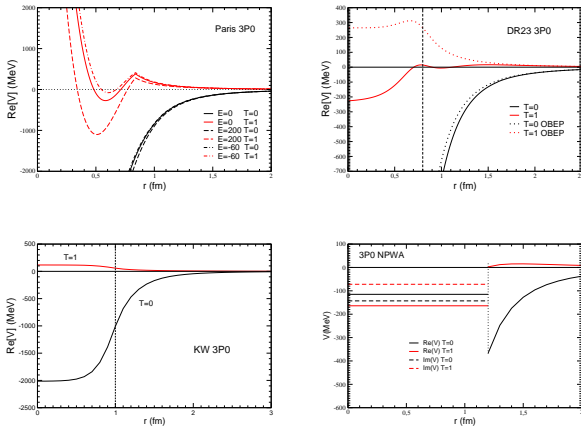


**Fig. 19** Real parts of  ${}^3P_0$  potentials for both isospins (T).

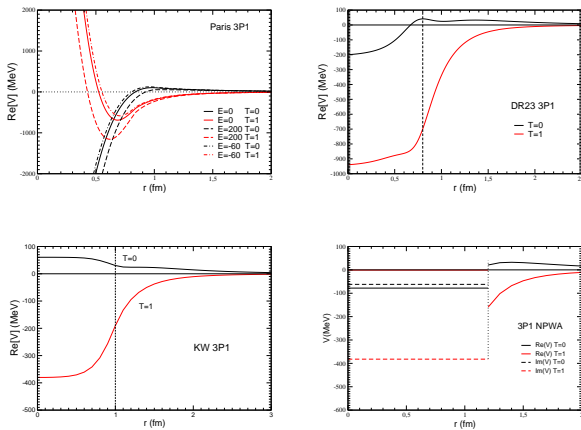


**Fig. 20** Real parts of  ${}^3P_1$  potentials for both isospins (T).

### ${}^3P_2$

The P-waves tensor coupled state is the one exhibiting the largest differences among models. The  ${}^3P_2$  component is attractive in both isospin states for all models but large differences in the strength are observed among them. The  ${}^3F_2$  is attractive and huge in all models but vanishes in the NPWA. For T=1, the potential is repulsive in Paris 09 but attractive in all the other models: the unique case where NPWA requires an attraction stronger than in all other potentials

Concerning the  ${}^3P_2 \rightarrow {}^3F_2$  transition potentials, the same remarks as for  ${}^3SD_1$  partial wave are in place.

### References

1. C. B. Dover, T. Gutsche, M. Maruyama and Amand Faessler, Prog. Part. Nucl. Phys., 29, (1992) 87-173

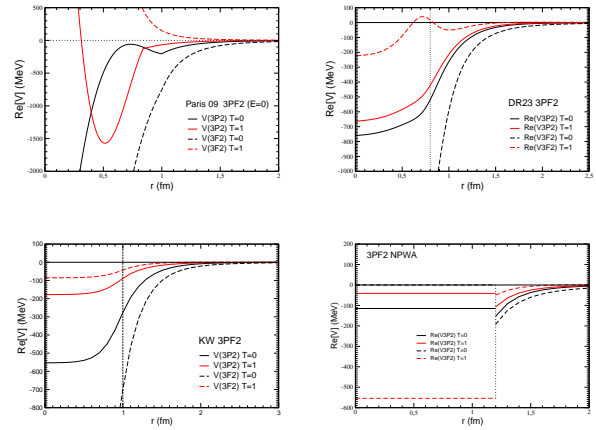


**Fig. 21** Real parts of  ${}^3P_2$  and  ${}^3F_2$  potentials for both isospins (T).

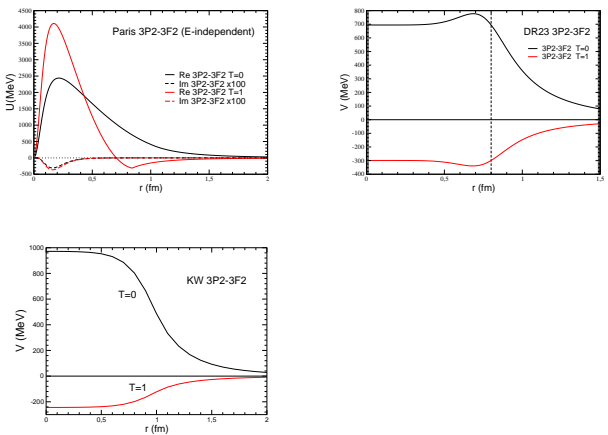


**Fig. 22**  ${}^3P_2 \rightarrow {}^3F_2$  transition potentials for both isospins (T). In DR and KW models, they are real.

2. E. Klempt, F. Bradamante, A. Martin, J.M. Richard, Phys Rep 368 (2002) 119
3. E. Klempt, Ch. Batty, J.M Richard, Phys Rep 413 (2005) 197-317
4. M. Levy, Nuovo Cimento VIII, 1 (1958) 92-134
5. J.M. Richard, Front. Phys. 8 (2020) 6, and references therein
6. J.M. Richard, Handbook of Nuclear Physics, Springer, 2022, I. Tanihata, H. Toki and T. Kajino, Eds.
7. Daren Zhou and Rob G. E. Timmermans, Phys. Rev. C 86, 044003 (2012)
8. M. C. M. Rentmeester, R. G. E. Timmermans, J. L. Friar, and J. J. de Swart, Phys. Rev. Lett. 82, 4992 (1999).
9. M. C. M. Rentmeester, R. G. E. Timmermans, and J. J. de Swart, Phys. Rev. C 67, 044001 (2003).
10. J.M. Richard, Phys Rev C (1995) 52:1143?4
11. Xian-Wei Kang, Johann Haidenbauer and Ulf-G. Meißner, JHEP 02 (2014) 113
12. Ling-Yun Dai, Johann Haidenbauer, Ulf-G. Meißner, JHEP 1707 (2017) 078
13. T. Hippchen, J. Haidenbauer, K. Holinde, and V. Mull Phys. Rev. C 44 (1991) 1323 V. Mull, J. Haidenbauer, T. Hippchen and K. Holinde, Phys. Rev. C 44 (1991) 1337

14. E. Epelbaum, H. Krebs and U.-G. Meißner, Eur. Phys. J. A 51 (2015) 53
15. PUMA, antiProton unstable matter annihilation  
T. Aumann, W. Bartmann, O. Boine-Frankenheim, A. Bouvard, A. Broche, F. Butin, D. Calvet, J. Carbonell, P. Chiggiato, H. De Gerssem, R. De Oliveira, T. Dobers, F. Ehm, J. Ferreira Somoza, J. Fischer, M. Fraser, E. Friedrich, A. Frotscher, M. Gomez-Ramos, J.-L. Grenard, A. Hobl, G. Hupin, A. Husson, P. Indelicato, K. Johnston, C. Klink, Y. Kubota, R. Lazauskas, S. Malbrunot-Ettenauer<sup>3</sup>, N. Marsic, W. F. O Müller, S. Naimi, N. Nakatsuka, R. Necca, D. Neidherr, G. Neyens, A. Obertelli, Y. Ono, S. Pasinelli, N. Paul, E. C. Polacco, D. Rossi, H. Scheit, M. Schlaich, A. Schmidt, L. Schweikhard, R. Seki, S. Sels, E. Siesling, T. Uesaka, M. Vilén, M. Wada, F. Wienholtz, S. Wycech, S. Zacarias Eur. Phys. J. A (2022) 58:88
16. R. Lazauskas, J. Carbonell, Phys. Lett. B 820, 136573 (2021)  
P.-Y. Duerinck, R. Lazauskas, J. Carbonell, Phys. Lett. B 841 (2023) 137936
17. J. Carbonell, G. Ihle, J.M. Richard, Z. Phys. A 334 (1989) 329-341.
18. J. Carbonell, J.M. Richard and S. Wycech, Z. Phys. A 343 (1992) 325.  
A missprint is noticed in eq. (5) of this reference: the prefactor  $\left[\frac{1}{(2L+1)!!}\right]^2$  in the definition of  $g_L(\eta)$  should be removed and replaced by 1.
19. B. El-Bennich, M. Lacombe, B. Loiseau and S. Wycech, Phys. Rev. C 79, 054001 (2009)
20. C.B. Dover and J.M. Richard, Phys. Rev. C 21 (1980) 1466.
21. J.M. Richard, M.E. Sainio, Phys. Lett. B 110, 349 (1982)
22. M. Kohno, W. Weise, Nucl. Phys. A 454, 429 (1986)
23. Stephen Gasiorowicz., Elementary Particle Physics. Wiley, New York, 1966
24. B. Moussallam, PhD Thesis, Universite Paris VI, 1980 (unpublished).
25. J. Cote, M. Lacombe, B. Loiseau, B. Moussallam, R. Vinh Mau, Phys. Rev. Lett. 48, 1319 (1982)
26. M. Pignone, M. Lacombe, B. Loiseau, and R. Vinh Mau, Phys. Rev. C 50, 2710 (1994).
27. B. El-Bennich, M. Lacombe, B. Loiseau, and R. Vinh Mau, Phys. Rev. C 59, 2313 (1999)
28. M. Lacombe et al, Phys. Rev. D 12, 1495 (1975)
29. M. Lacombe, B. Loiseau, J.M. Richard, R. Vinh Mau, J. Côté , P. Pirès and R. de Toureil, Phys. Rev. C 21, 861 (1980)
30. T. Ueda, Prog. Th. Phys. 62 (1979) 1670
31. B. Moussallam, Z. Phys. A - Atomic Nuclei 325, 1-6 (1986)
32. R. A. Bryan, Phys. Rev. C 24, 2659 (1981)
33. S. Klarsfeld, Phys. Lett. B 126, 148 (1983)
34. R. A. Bryan, Phys. Rev. C 30, 305 (1984)
35. H.P. Stapp, T.J. Ypsilantis, N. Metropolis, Phys. Rev. 105 (1957) 302
36. J.-P. Dedonder, B. Loiseau, B. El-Bennich, S. Wycech, Phys. Rev. C 80, 045207 (2009)
37. J. P. Dedonder, B. Loiseau, S. Wycech, Phys. Rev. C 97 (2018) 065206
38. E. Ydrefors and J. Carbonell, Eur. Phys. J. A (2021) 57:303
39. S. K. Saha, D. R. Entem, R. Machleidt and Y. Nosyk, Phys. Rev. C 107, 034002 (2023)
40. N. Kaiser, R. Brockmann, W. Weise, Nucl. Phys. A 625 (1997) 758-788
41. J. Carbonell, O.D. Dalkarov, K.V. Protasov, I.S. Shapiro, Nucl. Phys. A 535(1991)651-668
42. Xian-Wei Kang, Johann Haidenbauer and Ulf-G. Meißner, Phys. Rev. D 91, 074003 (2015)
43. Ling-Yun Dai, Johann Haidenbauer and Ulf-G. Meissner, Phys. Rev D 98, 014005 (2018)
44. Benoît Loiseau, private communication
45. T.E.O Ericson and W. Weise, Pions and Nuclei, Oxford University Press (1988)
46. A. Bulgac, G.A. Miller, and M. Strikman, Phys. Rev. C 56, 3307 (1997)
47. T.L. Trueman, Nucl. Phys. 26, 57 (1961)
48. D. Gotta *et.al.*, Nucl. Phys. **A660**, 283(1999).
49. M. Augsberger et al, Nucl. Phys. A **658** (1999) 149.
50. D. Gotta, Prog. in Particle and Nuclear Phys. **52**, 133 (2004).